# The single electron response of NEWS-G Spherical Proportional Counters

Daniel Durnford

CAP Congress 2019
June 5th

UNIVERSITY OF ALBERTA

Spherical Proportional Counters (SPCs) to search for low-mass dark matter


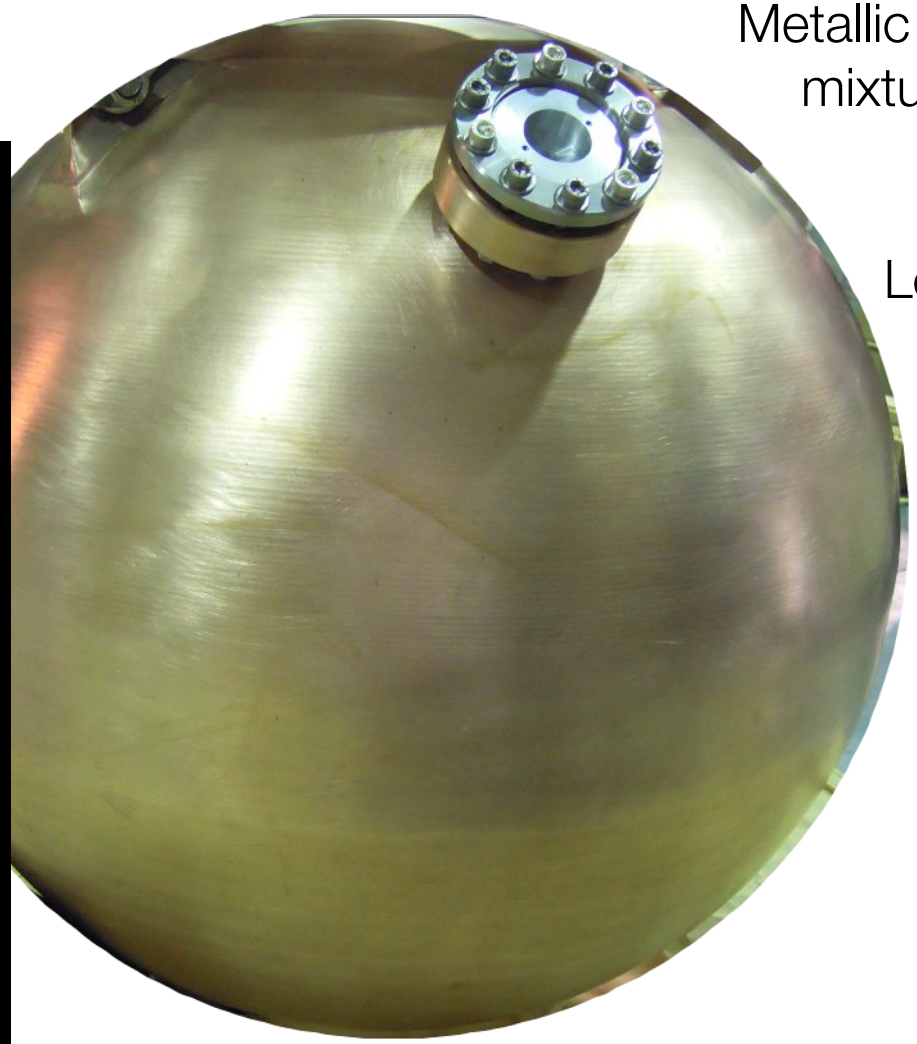

Metallic vessel filled with a noble gas mixture, with a single high voltage anode/sensor

Low-A target atoms increases sensitivity to low-mass WIMPs

1 GeV WIMP, different targets

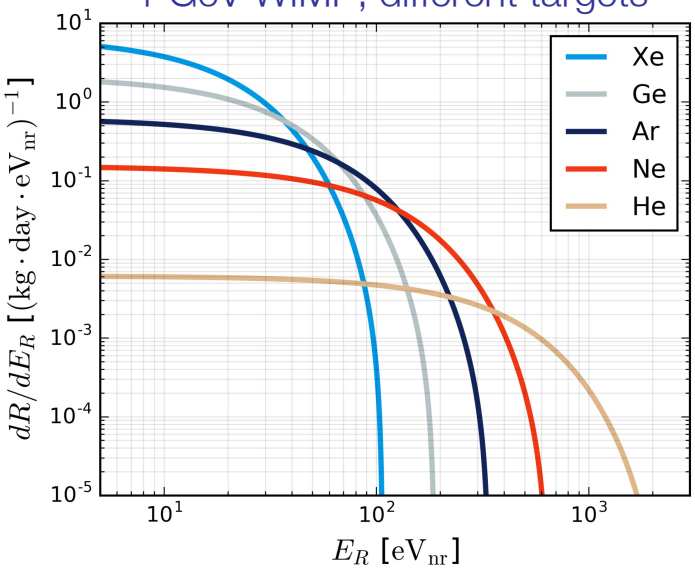

Spherical Proportional Counters (SPCs) to search for low-mass dark matter

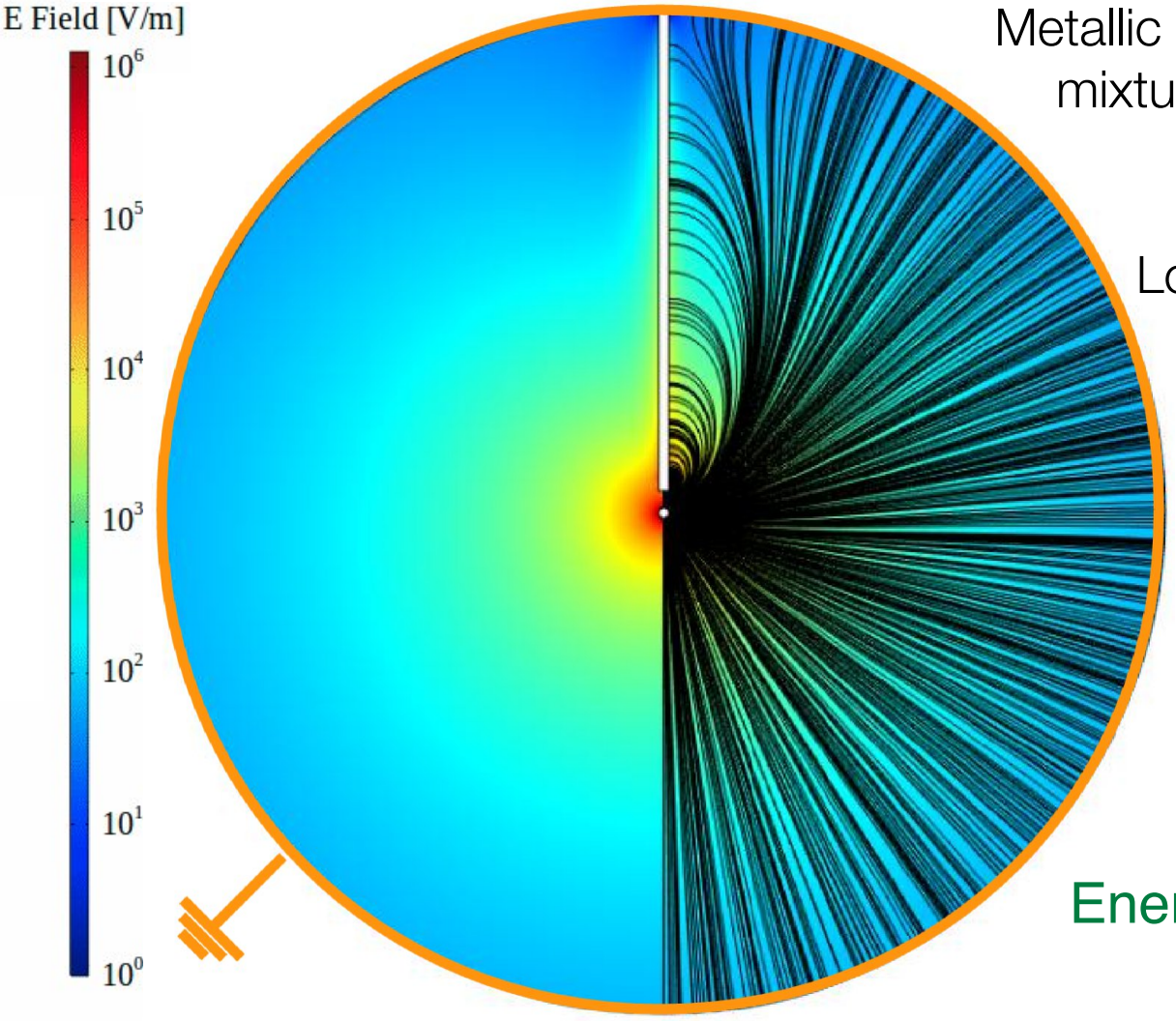


Metallic vessel filled with a noble gas mixture, with a single high voltage anode/sensor

Low-A target atoms increases sensitivity to low-mass WIMPs

Low intrinsic capacitance:
(C ≈ 0.3 pF)

High amplification gain from Townsend avalanche

Energy thresholds of ~10 eV!

# Preparing for NEWS-G @ SNOLAB

NEWS-G is preparing to install a new detector at SNOLAB

Expected to be sensitive to WIMP masses ~100 MeV using H-rich gas and an energy threshold < 50 eV

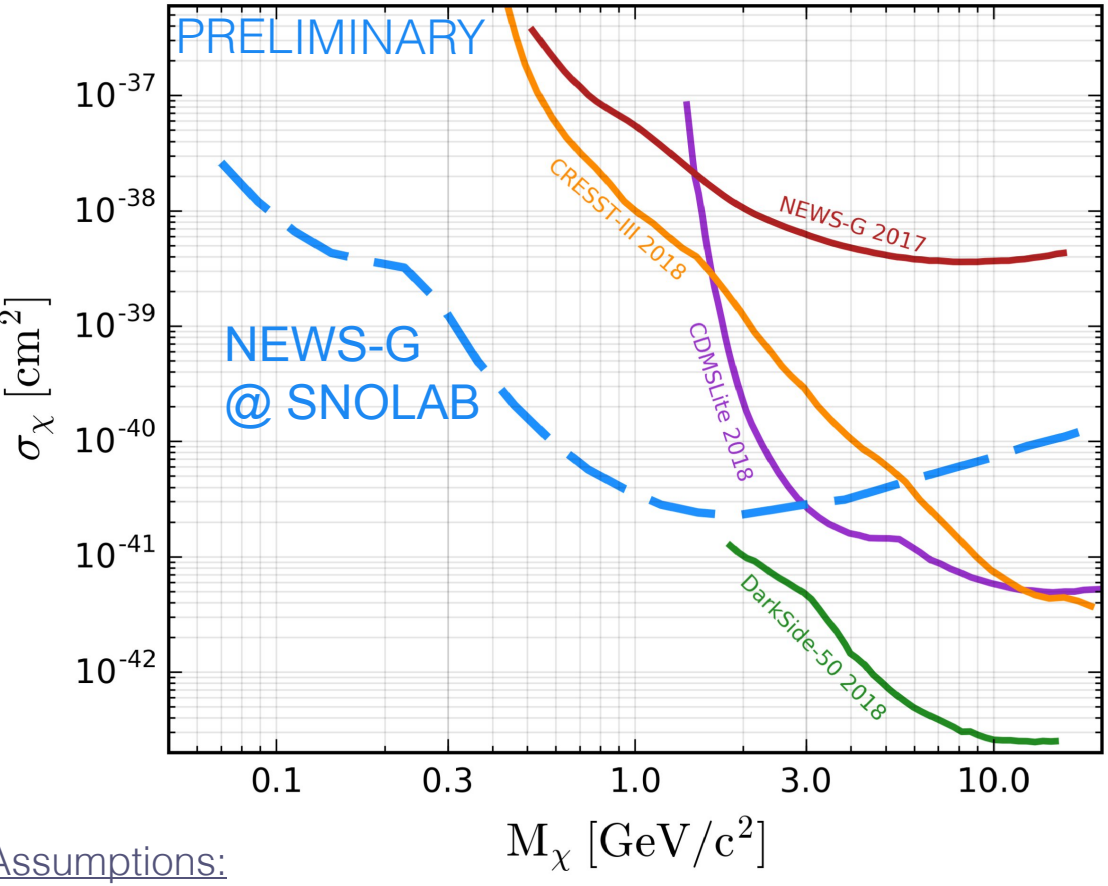


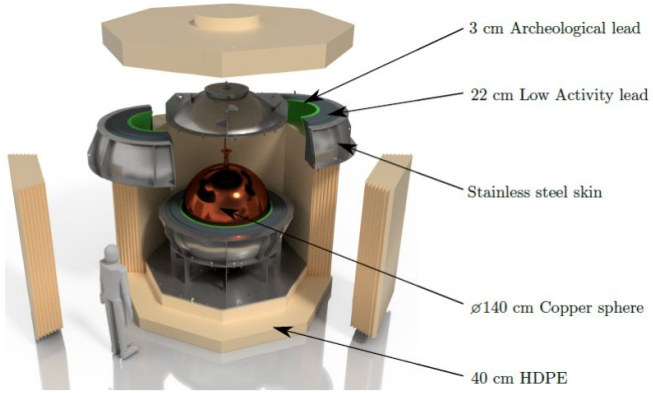



Assumptions:

Ne + 10% $CH_4$, Exposure: 20 kg days, F = 0.2, θ = 0.12,
SRIM quenching factor, Background: 1.78 dru, ROI: 14 $eV_{ee}$ - 1 $keV_{ee}$
Median of 500 MCs, Optimum Interval Method

Much of our sensitivity at these WIMP masses derives from $1e^-$ events:

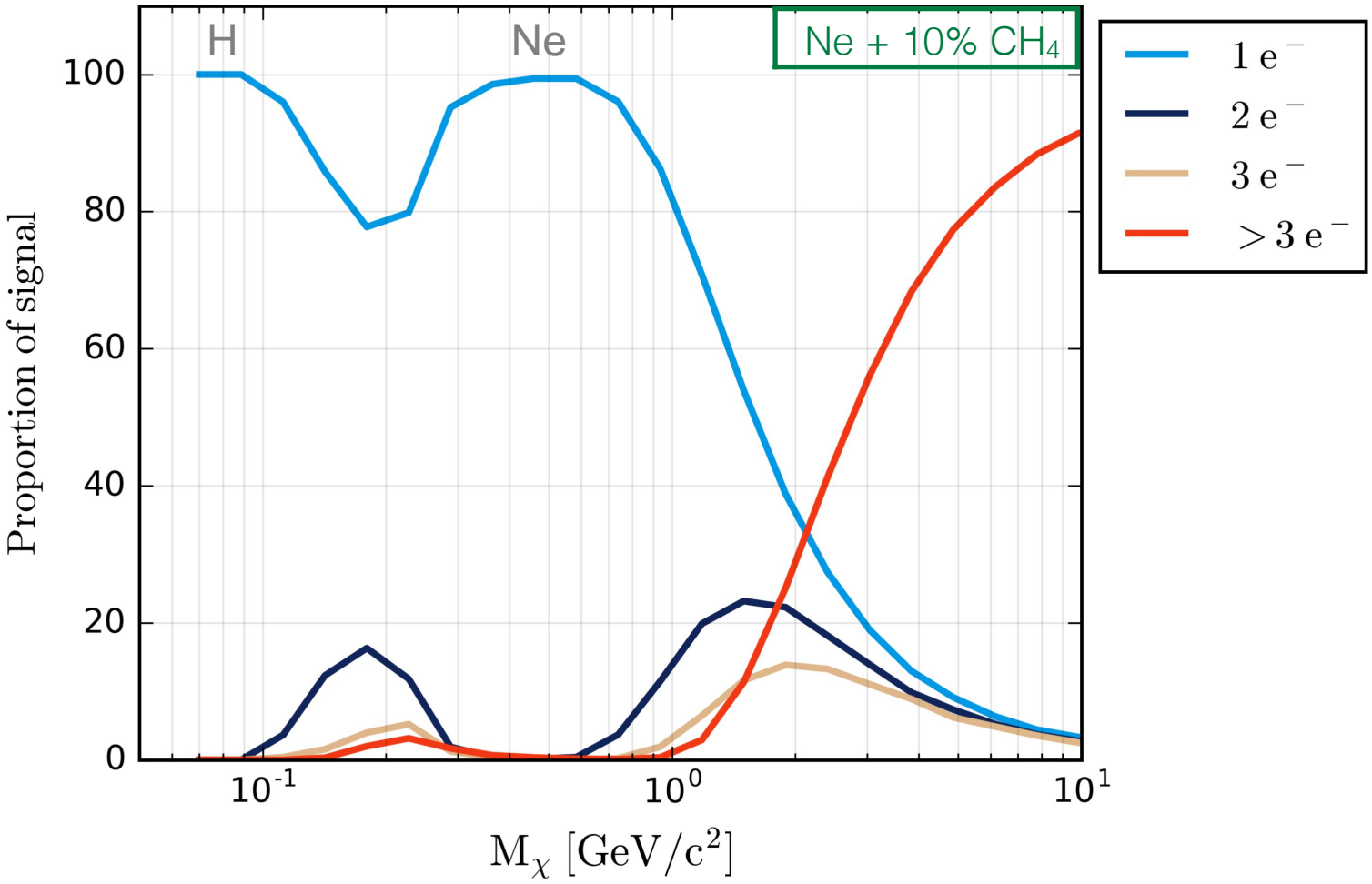


Therefore characterization of our single electron response is essential!

# What is our single-electron response?

The distribution of the number of avalanche pairs *"S"* is roughly exponential

It is known to be well-described by the Polya distribution, with shape parameter θ:

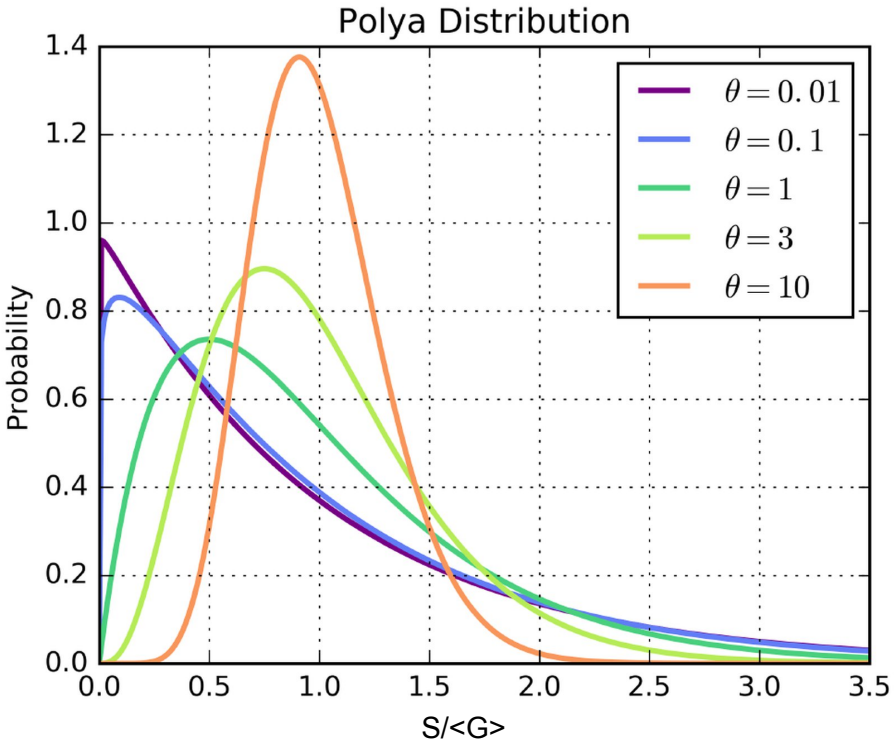


Visualisation of a Townsend Avalanche

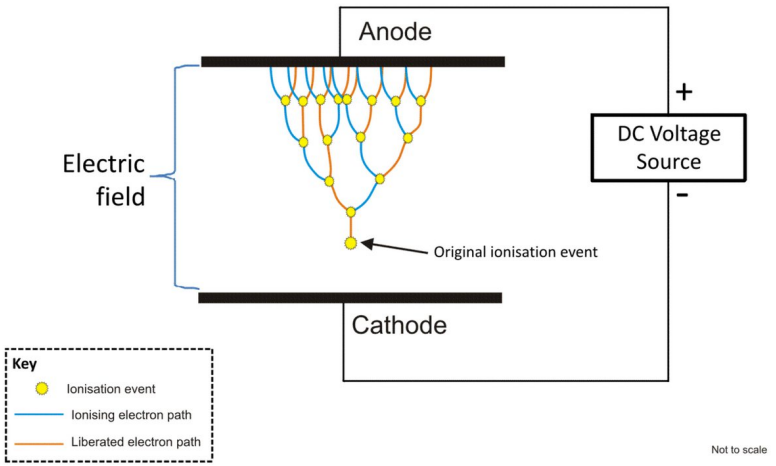


$$P_{\text{Polya}}\left(S|\left\langle G\right\rangle,\theta\right)=\frac{1}{\left\langle G\right\rangle}\left(\frac{\left(1+\theta\right)^{1+\theta}}{\Gamma\left(1+\theta\right)}\right)\times\left(\frac{S}{\left\langle G\right\rangle}\right)^{\theta}\exp\left(-\left(1+\theta\right)\frac{S}{\left\langle G\right\rangle}\right)$$


» J. Derré et al, NIM A 449, 314 - 321 (2000).
» T. Zerguerras et al, NIM A 608, 397 - 402 (2009).
» M. Kobayashi et al, NIM A 845, 236 - 240 (2017).
» R. Bellazzini et al, NIM A 581, 246 - 253 (2007).

# UV laser setup

Q. Arnaud et al. (NEWS-G Collaboration), *Precision laser-based measurements of the single electron response of spherical proportional counters for the NEWS-G light dark matter search experiment*, Phys. Rev. D 99, 102003 (2019)

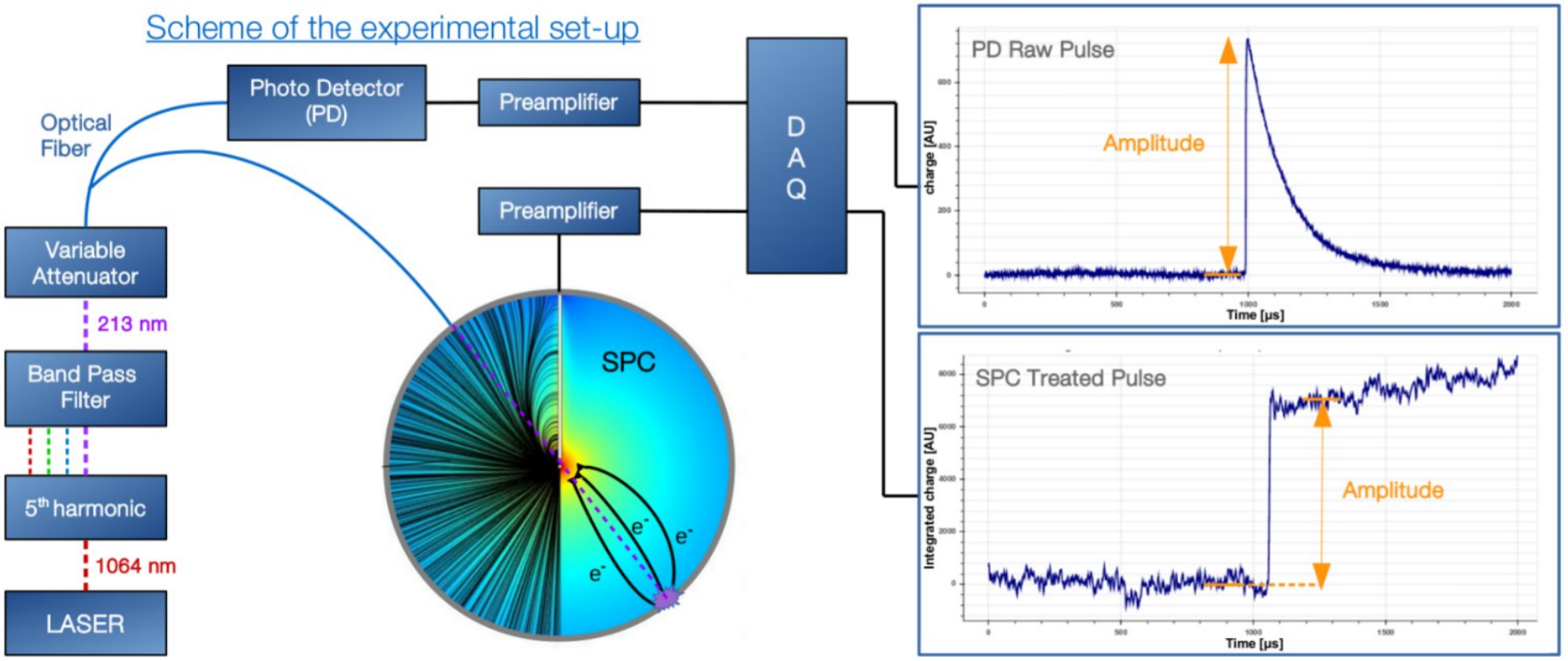

# UV laser setup

Tunable transmission to control the mean number of electrons

Common DAQ for timing analysis between two channels

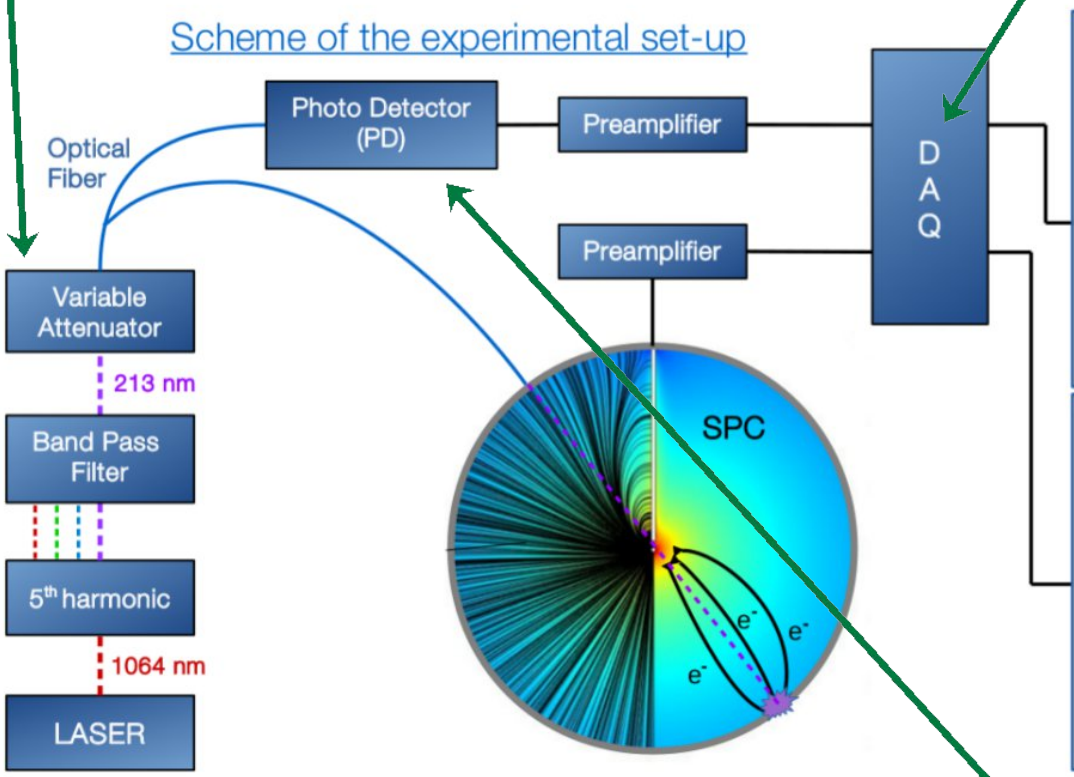


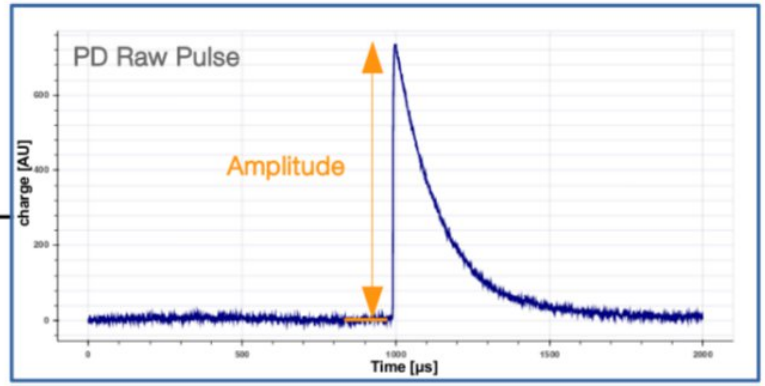


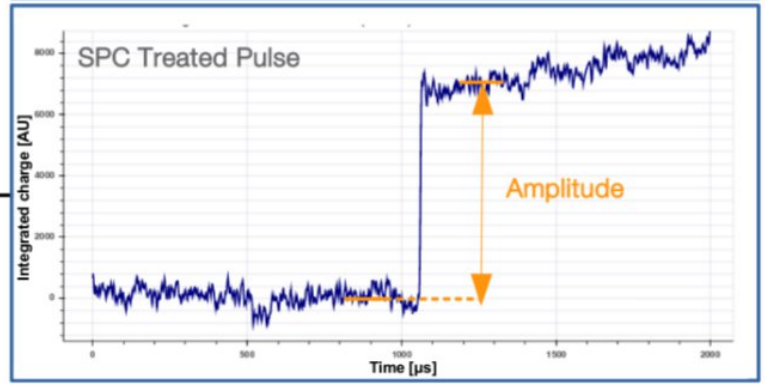


A powerful UV laser capable of extracting 100s of electrons

Parallel photo-detector to tag laser events

Q. Arnaud et al. (NEWS-G), Phys. Rev. D 99, 102003 (2019)

# Laser response model

*N* photo-electrons are extracted from the surface of the sphere: Poisson

$$P_{\text{Poisson}}(N|\mu) = \frac{e^{-\mu}\mu^N}{N!}$$

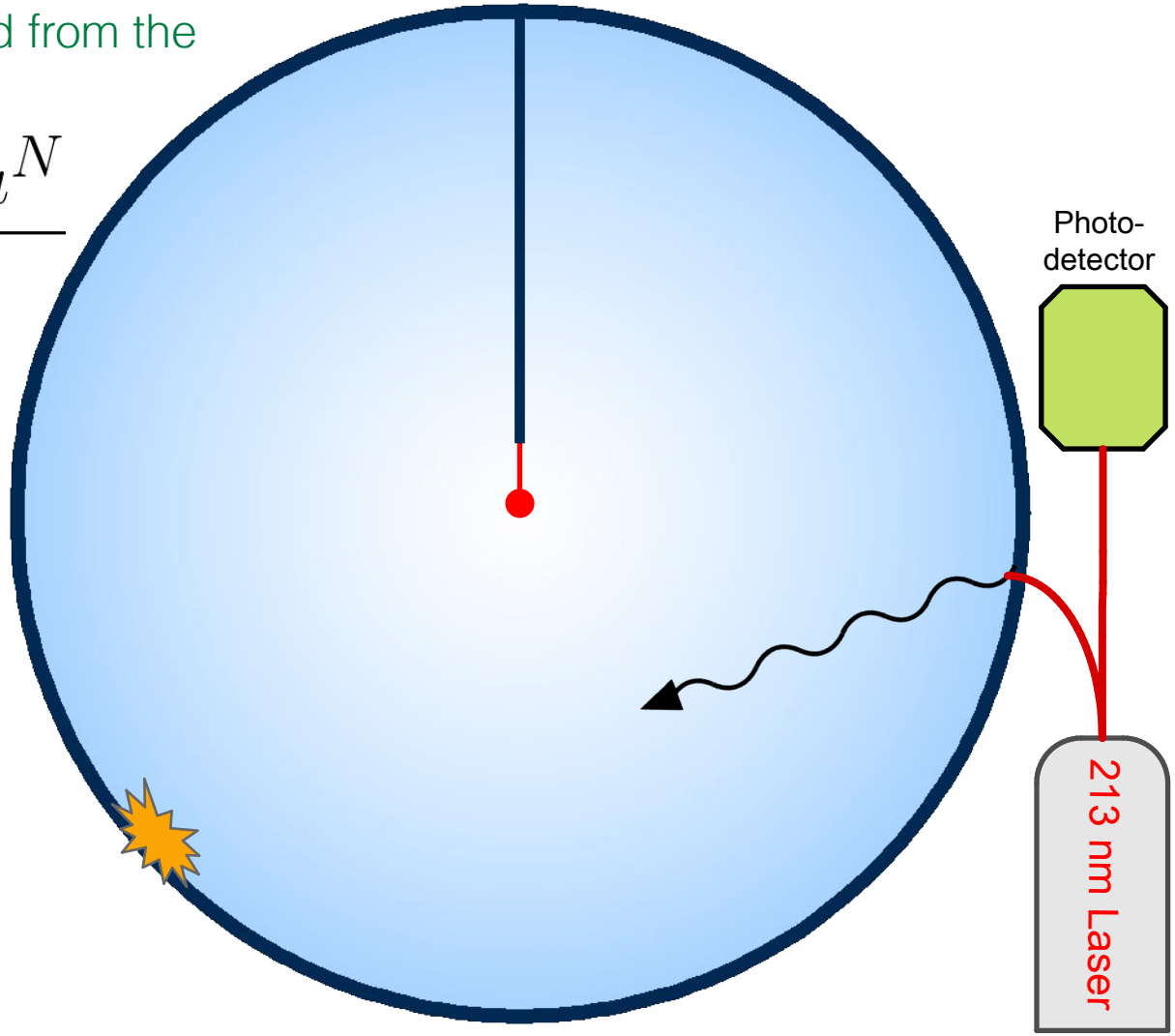

# Laser response model

*N* photo-electrons are extracted from the surface of the sphere: Poisson

The electrons drift/diffuse towards the anode

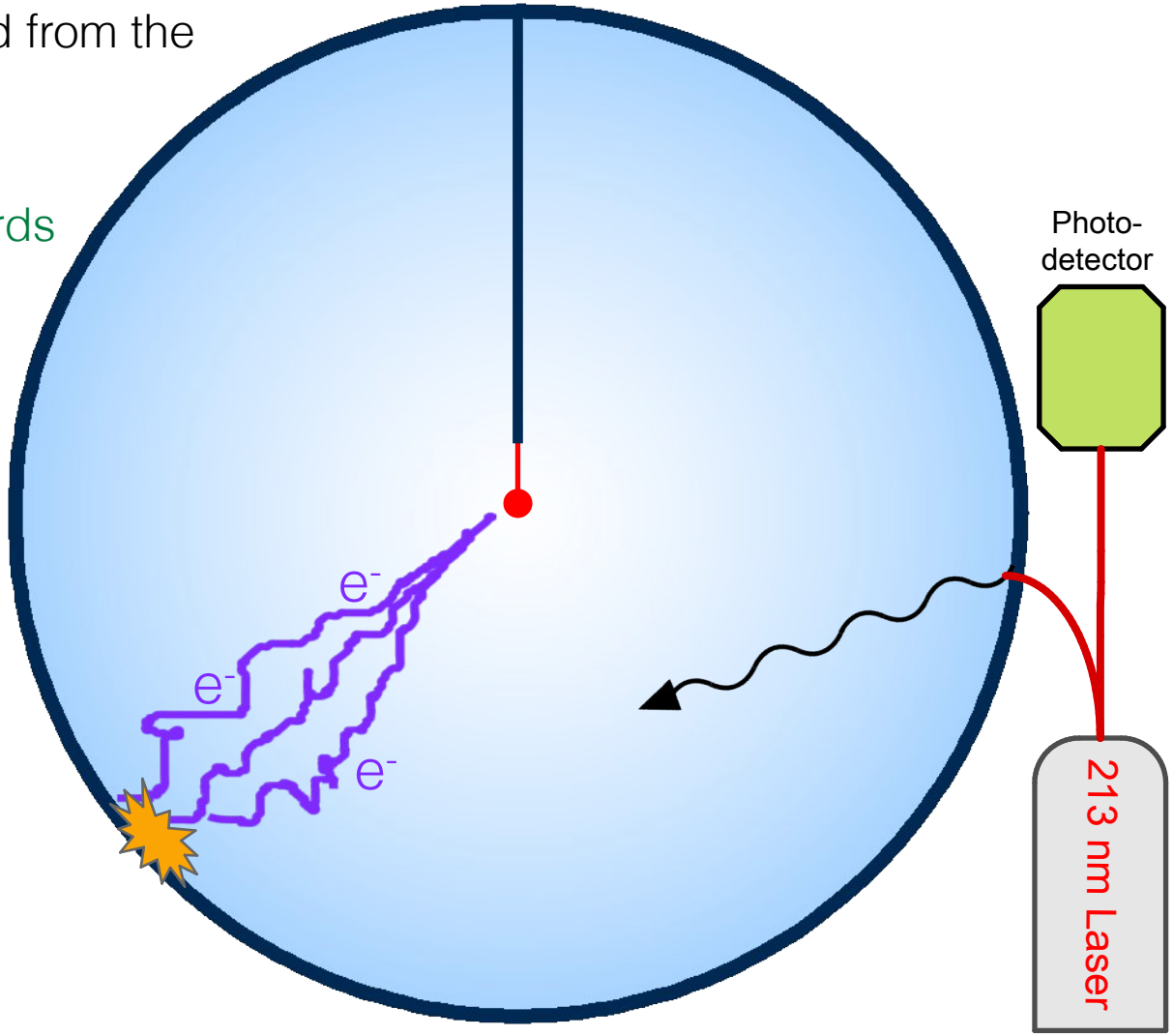

# Laser response model

*N* photo-electrons are extracted from the surface of the sphere: Poisson

The electrons drift/diffuse towards the anode

Each photo-electron creates *S* avalanche pairs:
N$^{th}$ convolution of Polya

If each avalanche is independent, then the overall avalanche response is the Nth convolution of the single-avalanche response

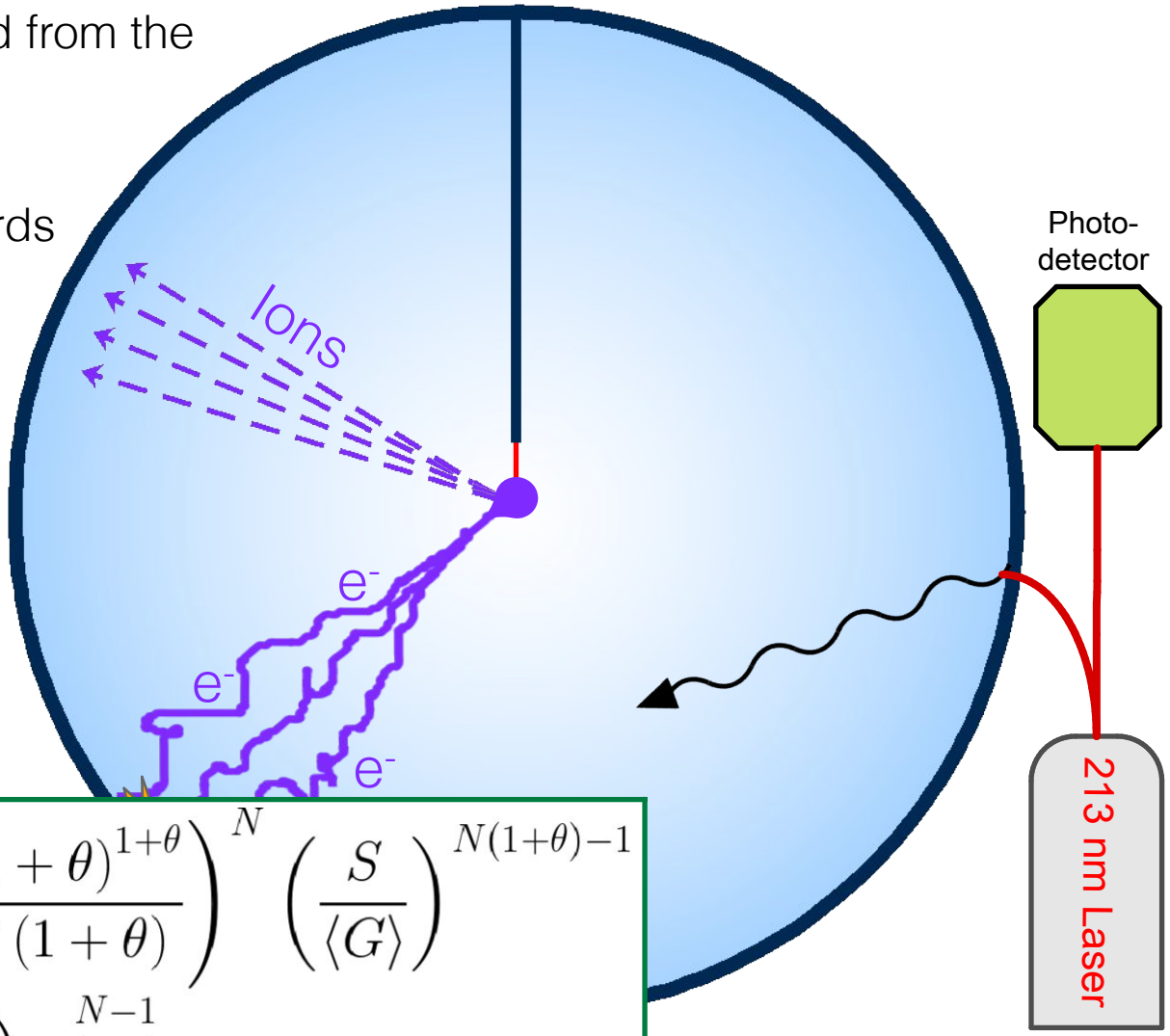


$$P^{(\mathrm{N})}_{\mathrm{Polya}}\left(S\middle|\langle G\rangle,\theta\right)=\frac{1}{\langle G\rangle}\left(\frac{(1+\theta)^{1+\theta}}{\Gamma(1+\theta)}\right)^{N}\left(\frac{S}{\langle G\rangle}\right)^{N(1+\theta)-1}$$
$$\times\exp\left(-(1+\theta)\left(\frac{S}{\langle G\rangle}\right)\right)\times\prod_{j=1}^{N-1}B\left((j+j\theta),(1+\theta)\right)$$

# Laser response model

*N* photo-electrons are extracted from the surface of the sphere: Poisson

The electrons drift/diffuse towards the anode

Each photo-electron creates *S* avalanche pairs:
N[th] convolution of Polya

Sum the contributions of all *N* photo-electrons

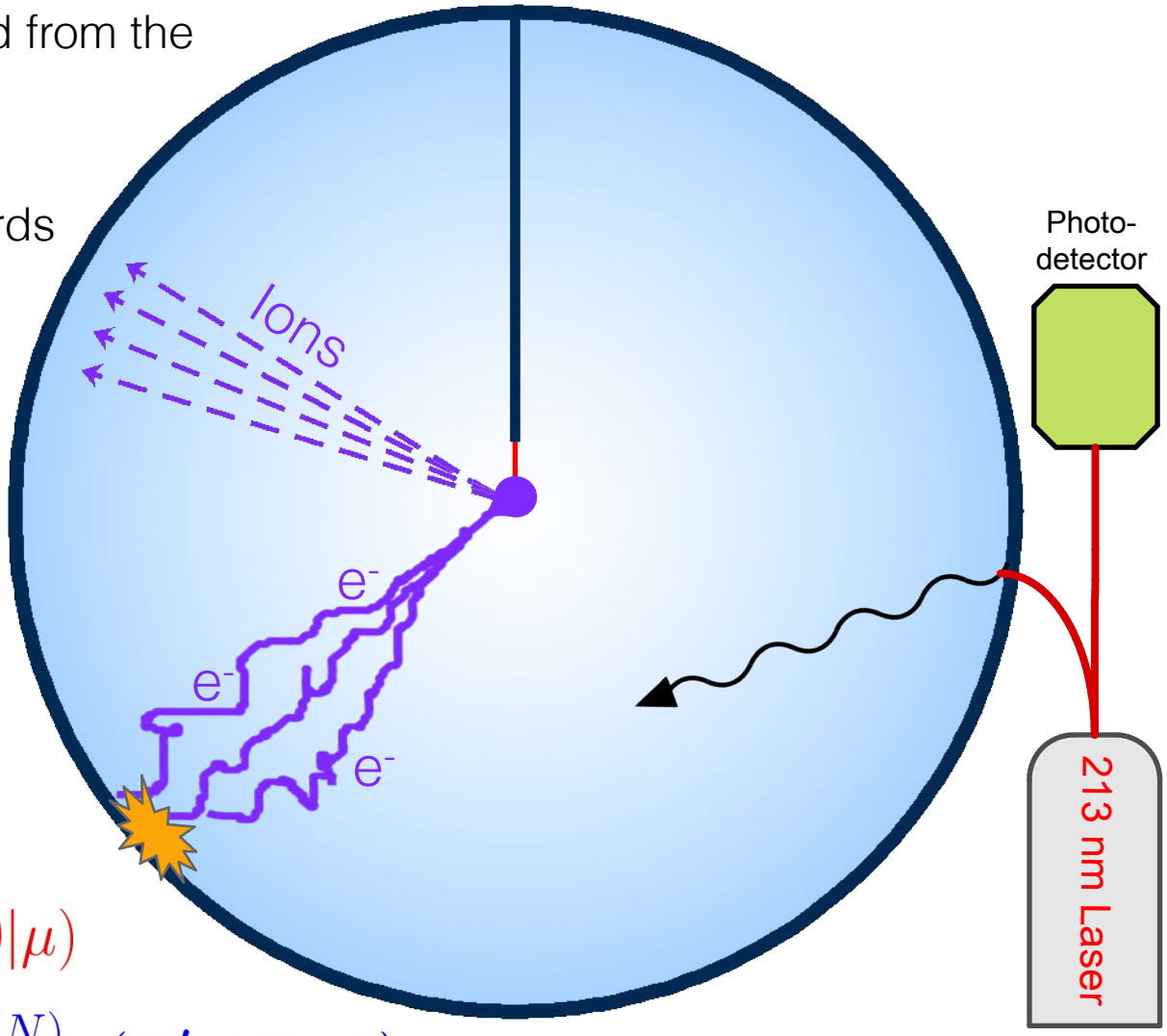


$$f\left(E'\right) = P_{\text{Poisson}}\left(N=0|\mu\right) + \sum_{N=1}^{\infty} P_{\text{Poisson}}\left(N|\mu\right) \times P_{\text{Polya}}^{(N)}\left(E'|\left\langle G\right\rangle,\theta\right)$$

# Laser response model

*N* photo-electrons are extracted from the surface of the sphere: Poisson

The electrons drift/diffuse towards the anode

Each photo-electron creates *S* avalanche pairs:
$N^{th}$ convolution of Polya

Sum the contributions of all *N* photo-electrons

The overall response is convolved with a Gaussian to model baseline noise

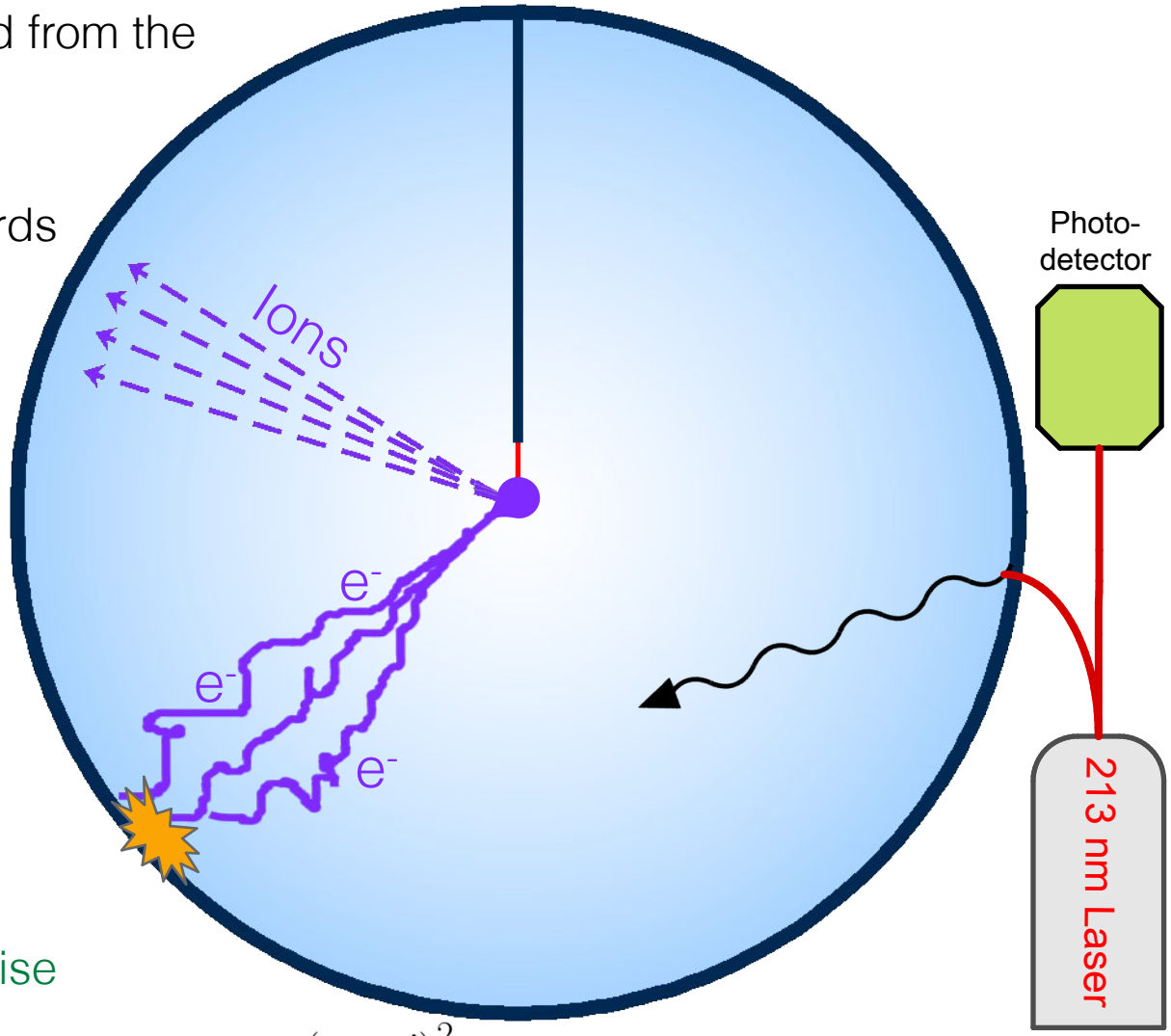


$$\mathcal{P}\left(E|\mu,\langle G\rangle,\theta,\sigma\right)=\frac{1}{\sqrt{2\pi\sigma^2}}\int_{-\infty}^{\infty}f\left(E'\right)e^{\frac{-\left(E-E'\right)^2}{2\sigma^2}}dE'$$

# Single electron response characterization

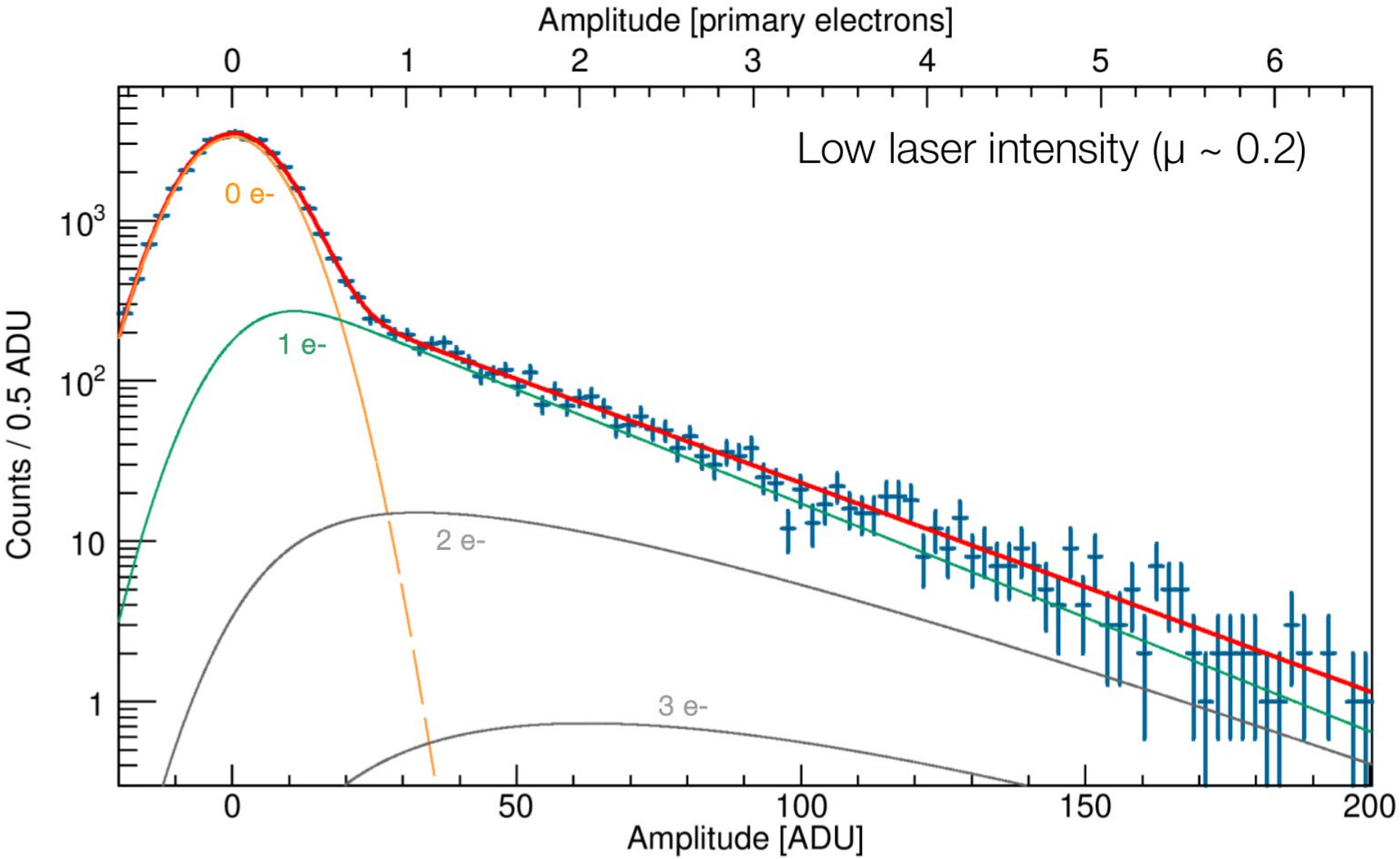


Q. Arnaud et al. (NEWS-G), Phys. Rev. D 99, 102003 (2019)

# Single electron response characterization

The excellent fit validates the response model. Binned log-likelihood:

$$\mathcal{L}\left(\mathbf{n}\middle|\left\langle\mathbf{G}\right\rangle,\theta,\sigma,\mu\right)=-\mu\sum_{i=1}^{n_{\mathrm{bins}}}n_i\log\left(n_{\mathrm{Total}}\int_{\Delta_i}\mathcal{P}\left(E'\right)dE'\right)$$

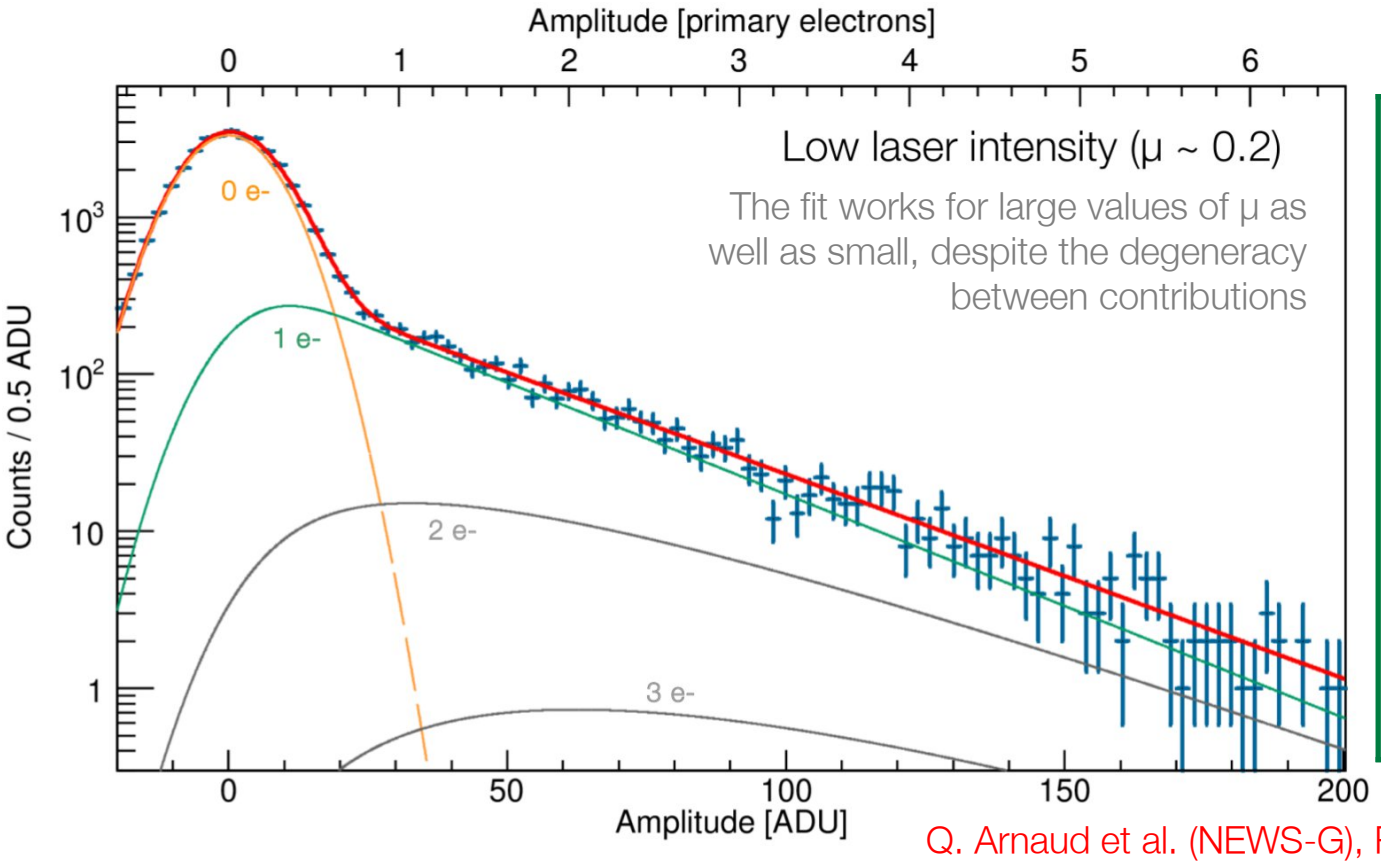


**Data Parameters:**

Ne + 2% CH4
P = 1.5 bar
HV = 1200V

**Fit results:**

θ = 0.09 ±0.02
<G> = 30.26 ± 0.21 ADU
$\chi^2$/ndf = 0.97

Q. Arnaud et al. (NEWS-G), Phys. Rev. D 99, 102003 (2019)

# Single electron response characterization

The excellent fit validates the response model. Binned log-likelihood:

$$\mathcal{L}\left(\mathbf{n}\middle|\left\langle\mathbf{G}\right\rangle,\theta,\sigma,\mu\right)=-\mu\sum_{i=1}^{n_{\mathrm{bins}}}n_i\log\left(n_{\mathrm{Total}}\int_{\Delta_i}\mathcal{P}\left(E'\right)dE'\right)$$

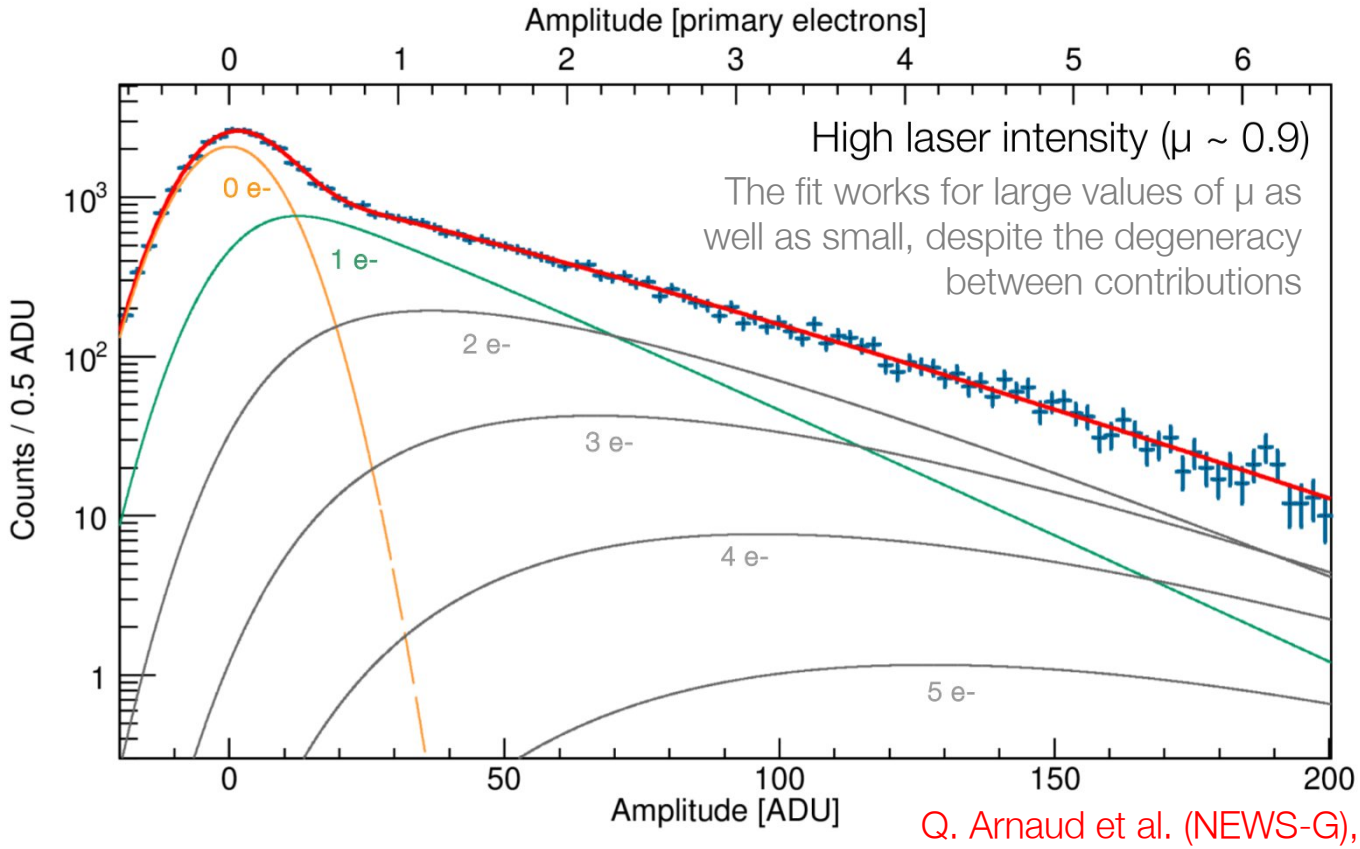


**Data Parameters:**

Ne + 2% CH4
P = 1.5 bar
HV = 1200V

**Fit results:**

θ = 0.09 ±0.02
<G> = 30.26 ± 0.21 ADU
$\chi^2$/ndf = 0.97

Q. Arnaud et al. (NEWS-G), Phys. Rev. D 99, 102003 (2019)

# Detector monitoring

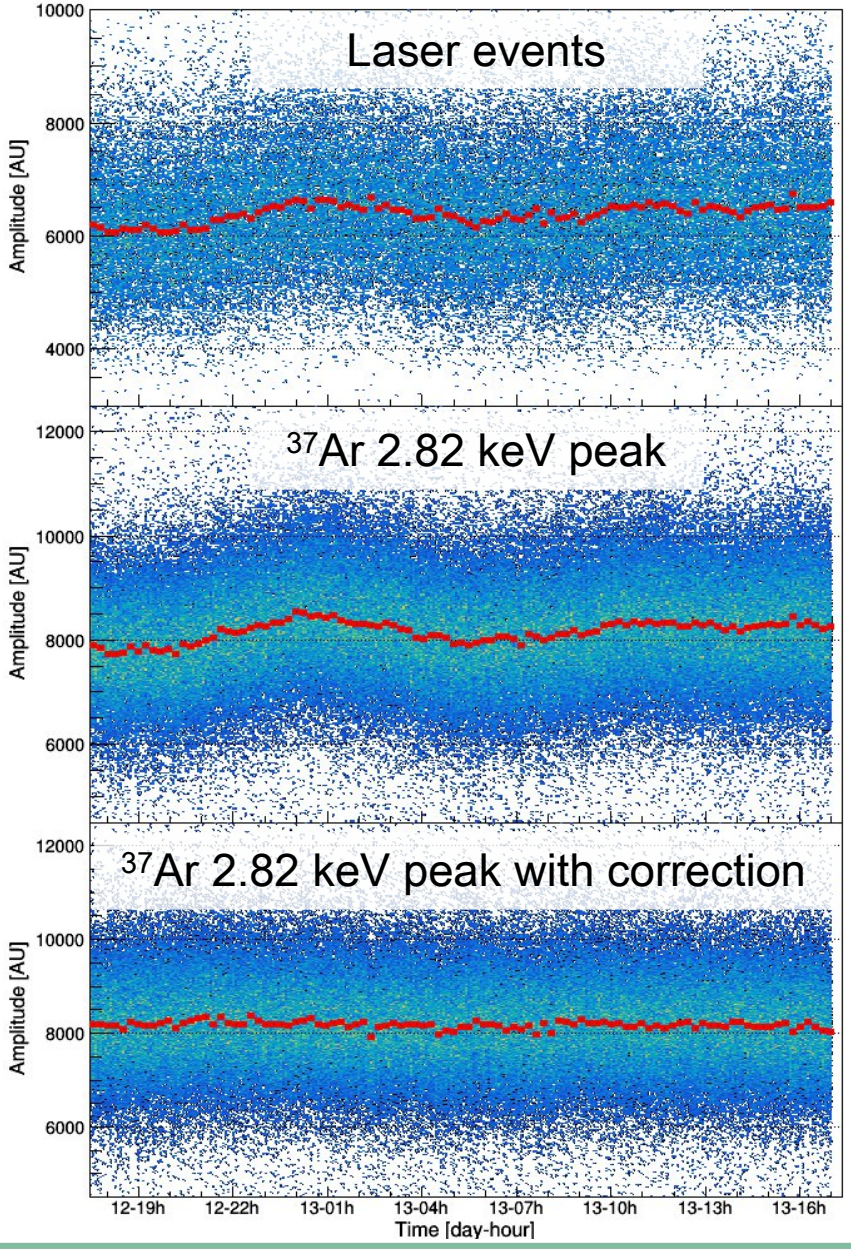


The laser can be used to monitor the detector response during physics runs

Long-term fluctuations in gain can be caused by temperature changes, $O_2$ contamination, sensor damage...

Laser monitoring data could even be used to correct for long-term fluctuations

Q. Arnaud et al. (NEWS-G), Phys. Rev. D 99, 102003 (2019)

# Electron drift time from sphere surface

The laser can measure the drift time and diffusion (dispersion in drift time) of surface electrons:

The drift time is time delay between photo-detector and SPC events

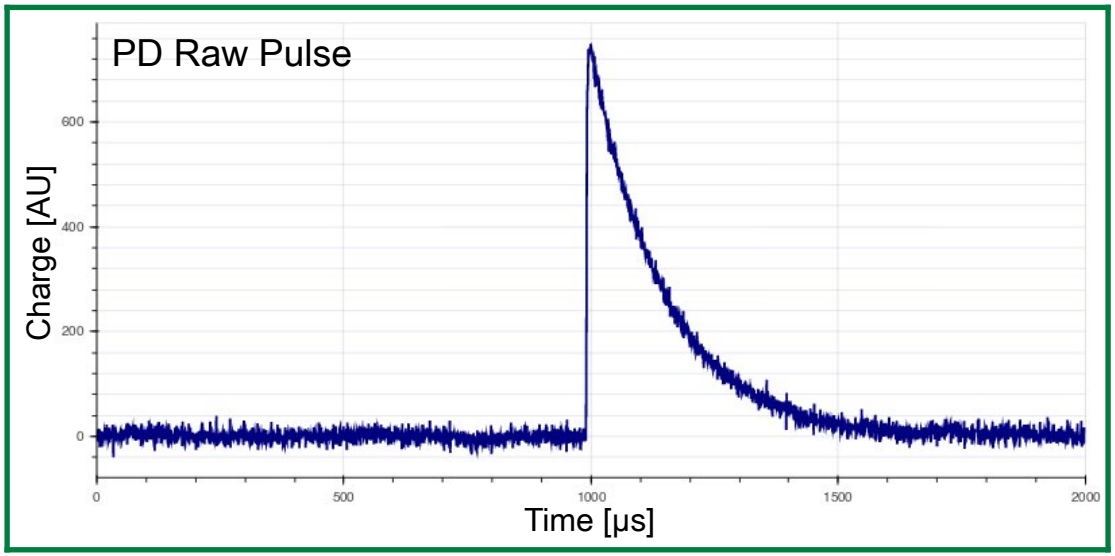


Drift time ~100 μs

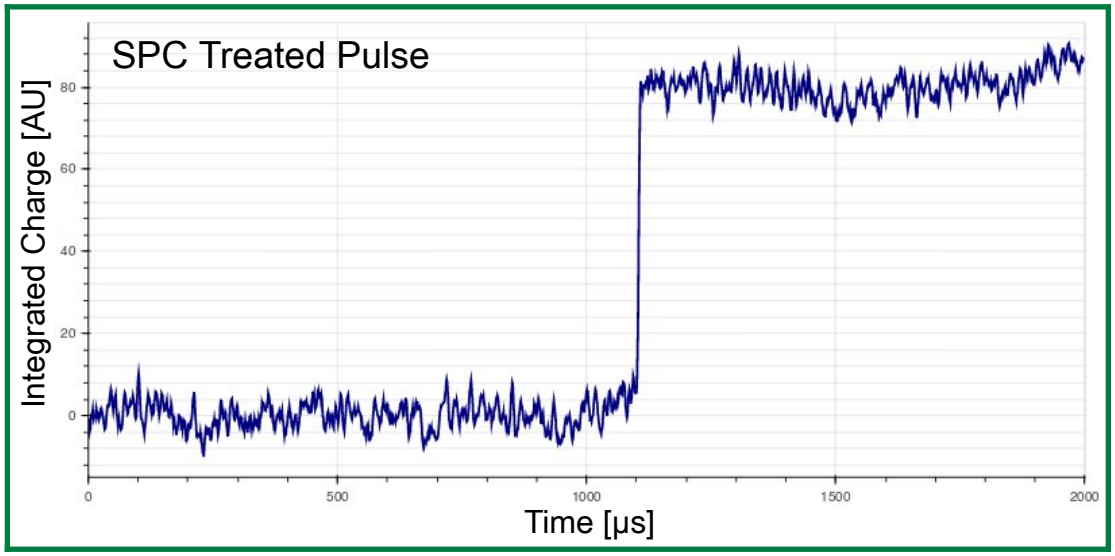

# Electron drift time from sphere surface

The laser can measure the drift time and diffusion (dispersion in drift time) of surface electrons:

The drift time is time delay between photo-detector and SPC events

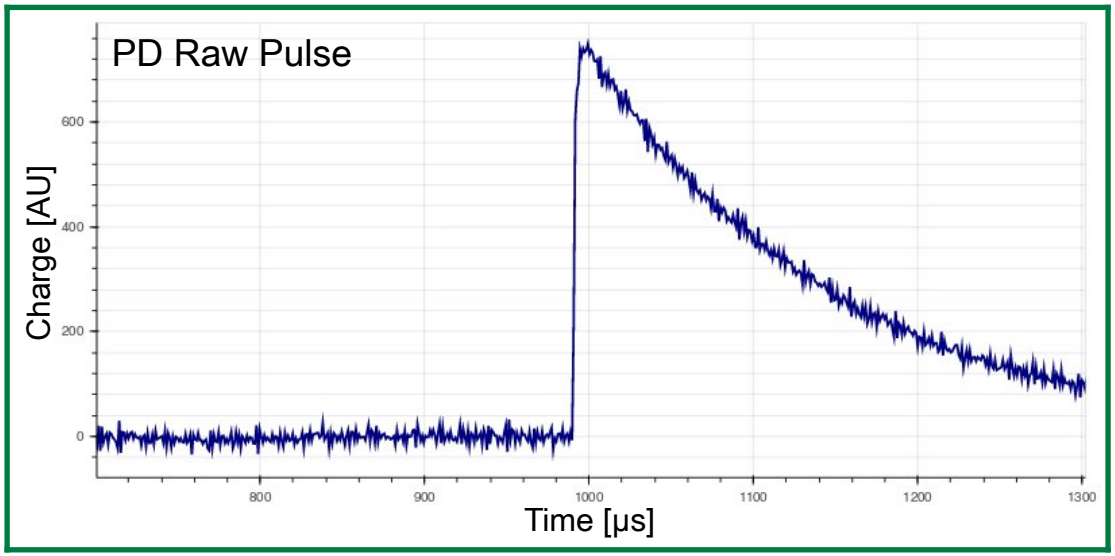


Drift time ~100 µs

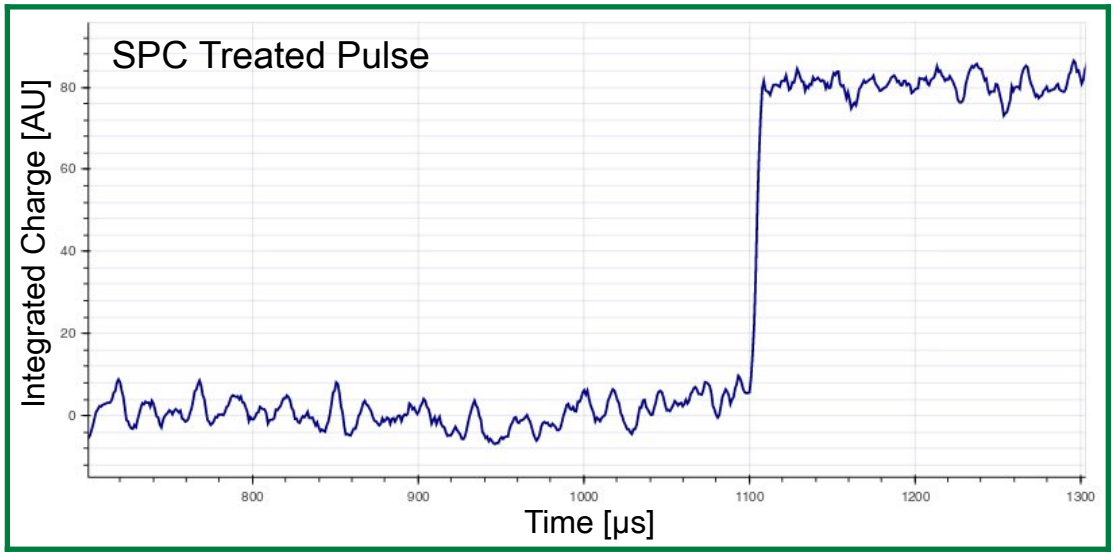

# Electron drift time from sphere surface

Q. Arnaud et al. (NEWS-G), Phys. Rev. D 99, 102003 (2019)

The laser can measure the drift time and diffusion (dispersion in drift time) of surface electrons:

The drift time is time delay between photo-detector and SPC events

Very sensitive to E-field structure, gas conditions

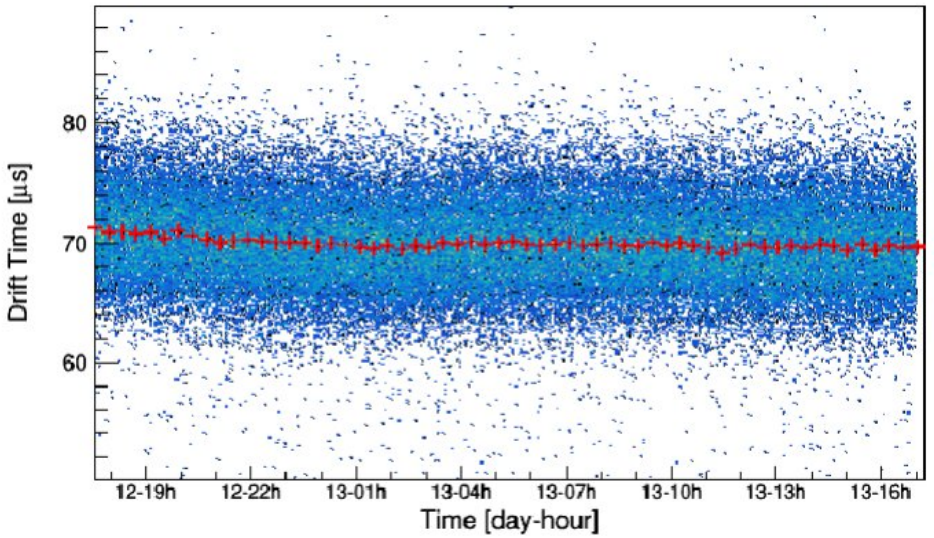

# Electron drift time from sphere surface

Q. Arnaud et al. (NEWS-G), Phys. Rev. D 99, 102003 (2019)

The laser can measure the drift time and diffusion (dispersion in drift time) of surface electrons:

The drift time is time delay between photo-detector and SPC events

Very sensitive to E-field structure, gas conditions

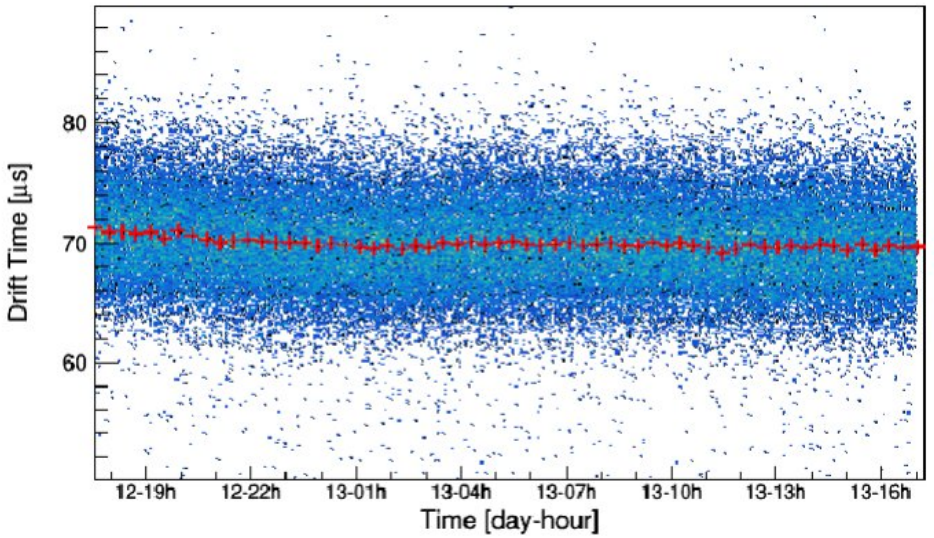


A way to validate electron transport simulations, monitor efficiency of fiducialization cuts

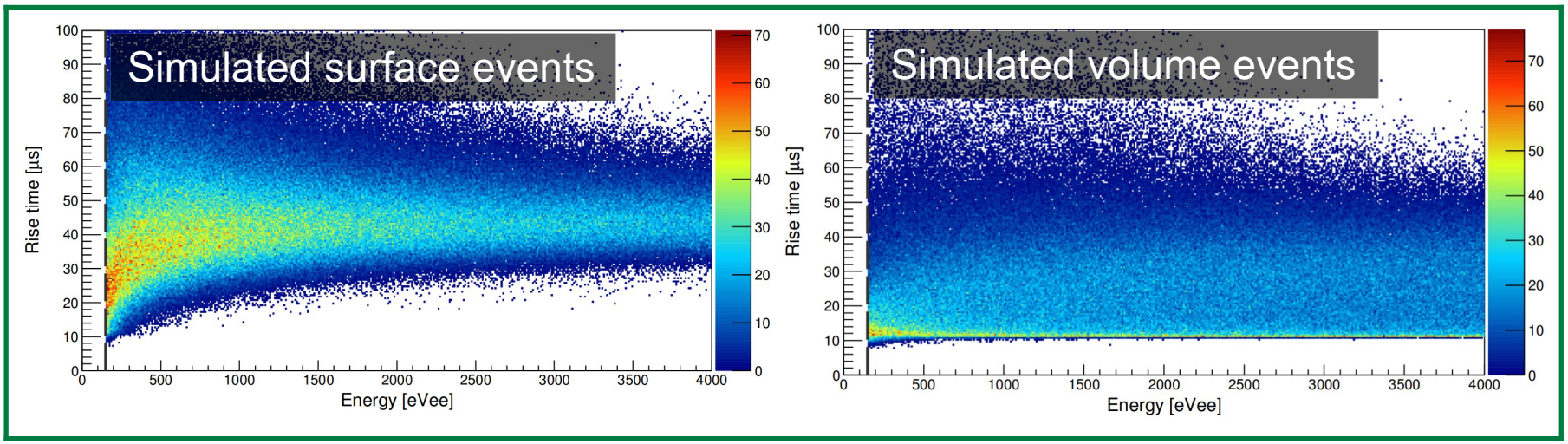


Q. Arnaud et al. (NEWS-G), Astropart. Phys. 97, 54 (2018)

# Trigger efficiency

The laser can be used to directly measure the efficiency of our triggering algorithm

**Method 1:**
SPC-triggered spectrum divided by photo-detector triggered spectrum (this does not account for null laser events)

**Method 2:**
Fit total spectrum (0 PE + > 0 PE events), then fit > 0 PE spectrum multiplied by error function with <G>, θ, and σ fixed.

Demonstration of ~10 eV energy threshold:
16 eV in this example

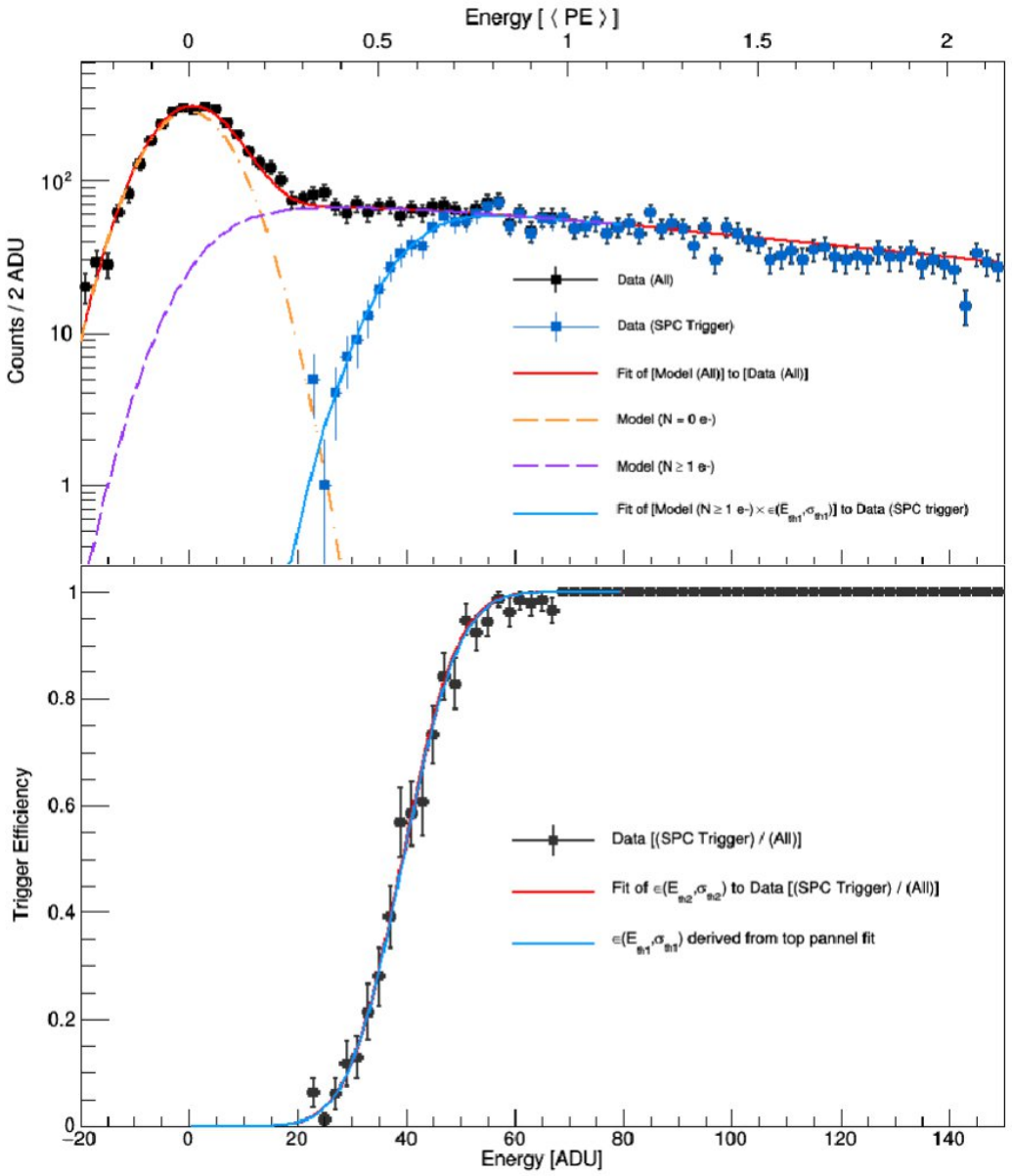


Q. Arnaud et al. (NEWS-G), Phys. Rev. D 99, 102003 (2019)

# $^{37}$Ar measurements

$^{37}$Ar gas was also injected into the SPC, produced in collaboration with the Royal Military College of Canada with a SLOWPOKE-2 reactor:
D.G. Kelly et al, J. Radioanal. Nucl. Chem. 318, 279 (2018)

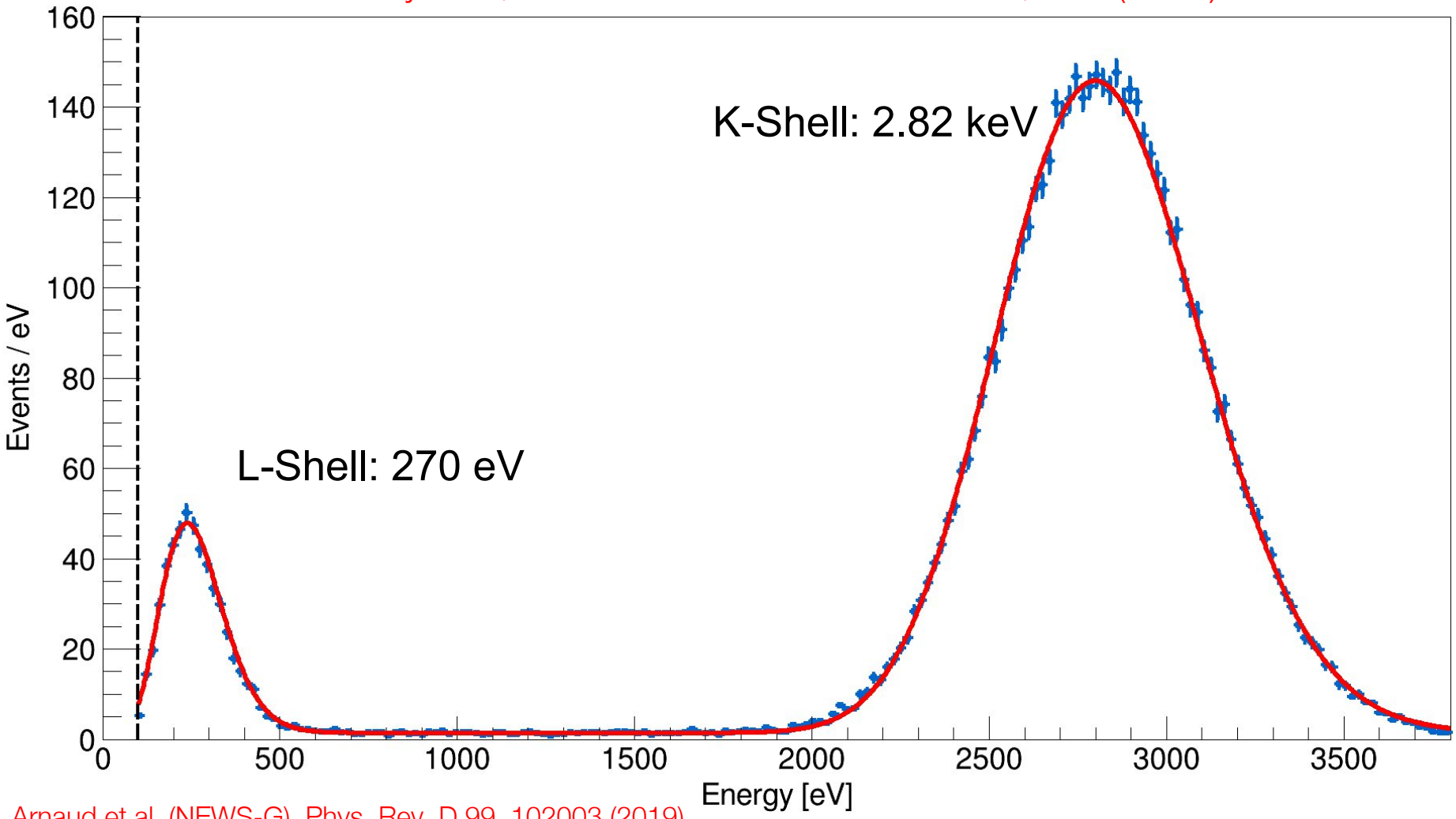


Q. Arnaud et al. (NEWS-G), Phys. Rev. D 99, 102003 (2019)

# $^{37}$Ar measurements

A test of our model for primary ionization -
D. Durnford et al, Phys. Rev. D 98, 103013 (2018)

$$f\left(E'\right) = \sum_{N=1}^{N_{\max}} P_{\mathrm{CMP}}\left(N|\mu, F\right) \times P_{\mathrm{Polya}}^{(\mathrm{N})}\left(E'|\left\langle G\right\rangle, \theta\right)$$

Also allowed for measurements of the W-value, Fano factor of this gas mixture at different energies:

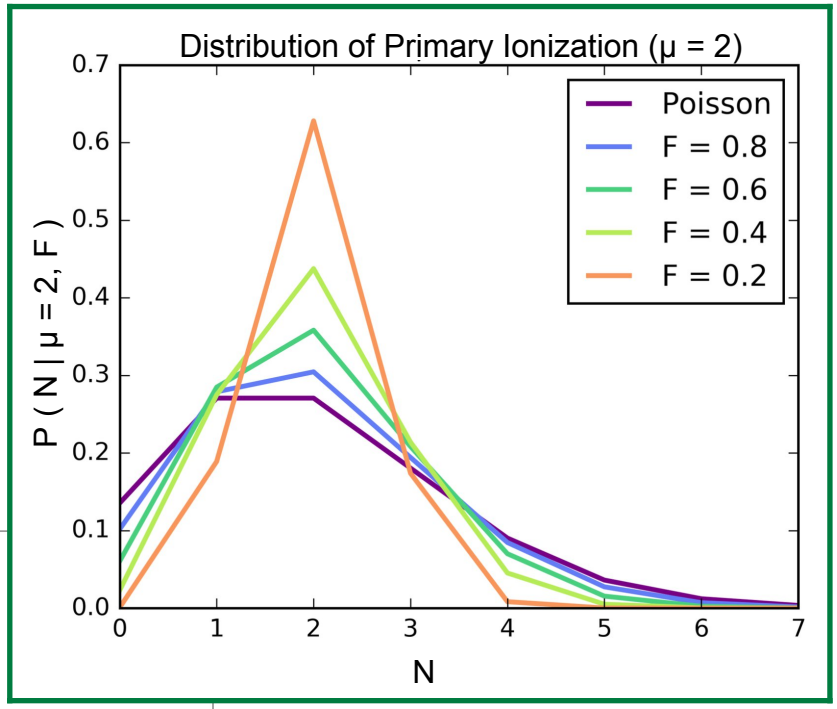


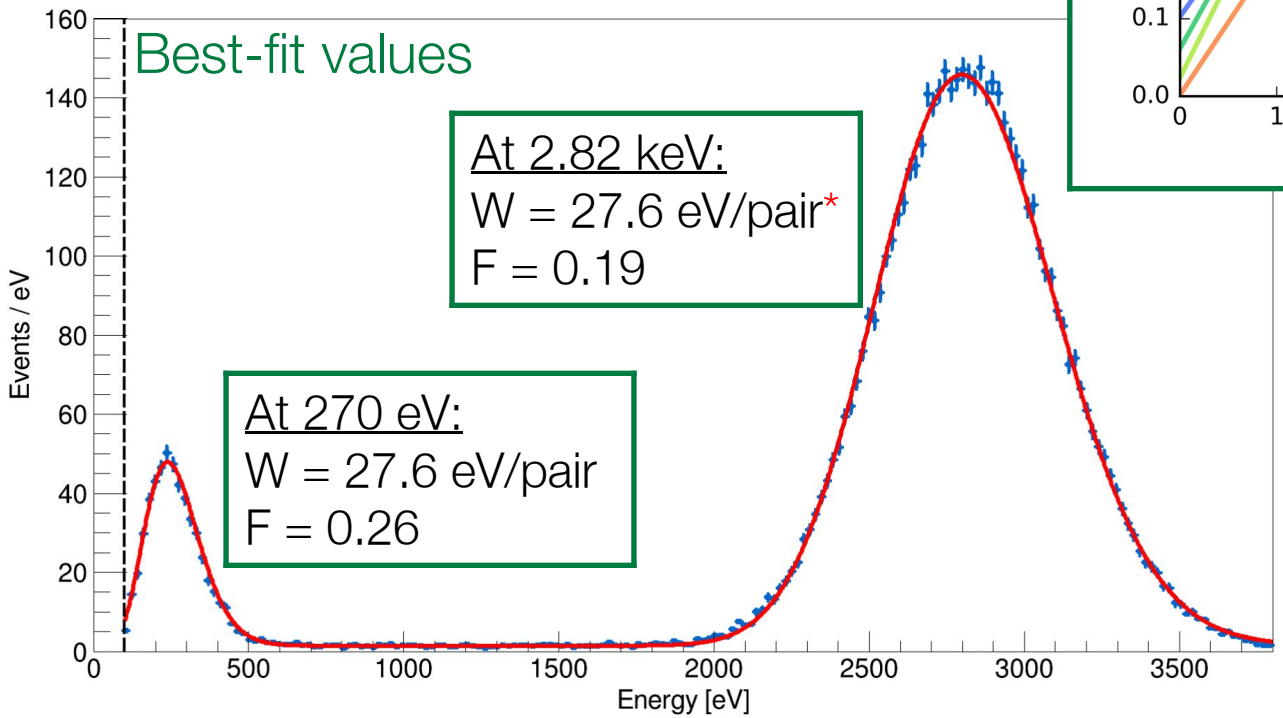


*The W-value at 2.82 keV was calculated directly from <G> and fixed for this fit

# Future work

In addition to playing a crucial role with NEWS-G at SNOLAB...

- The laser + $^{37}$Ar will be used to carry out extensive measurement campaigns of W-values and Fano factors for different gas mixtures, pressures, at multiple energies

- An aim-able laser fiber would allow direct validation of our finite-element simulations of sphere field structure

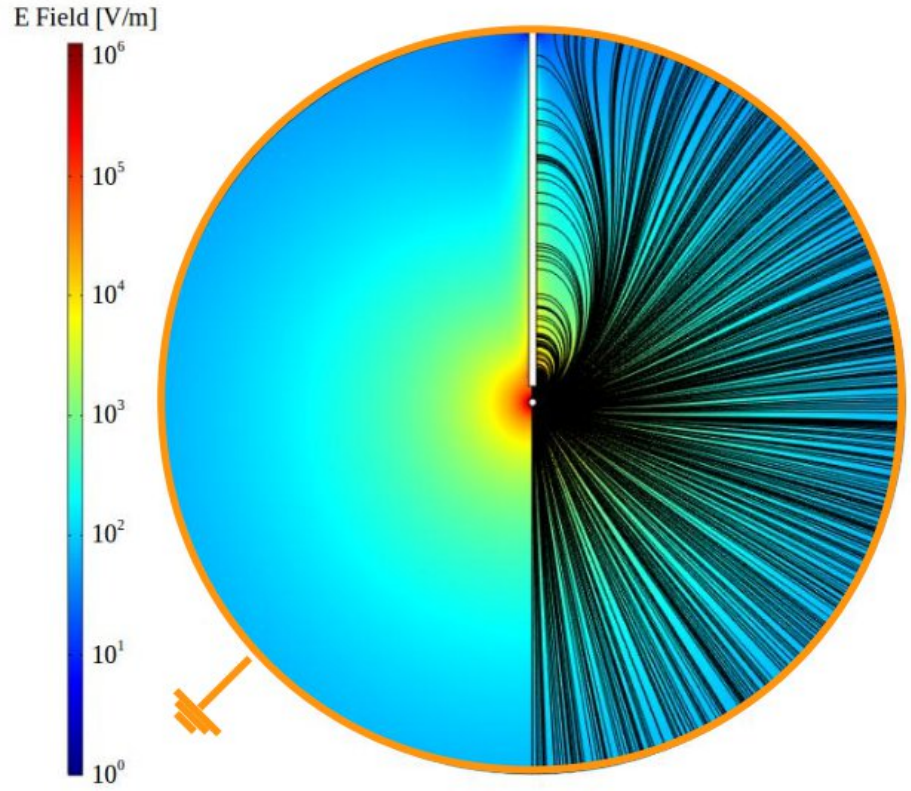


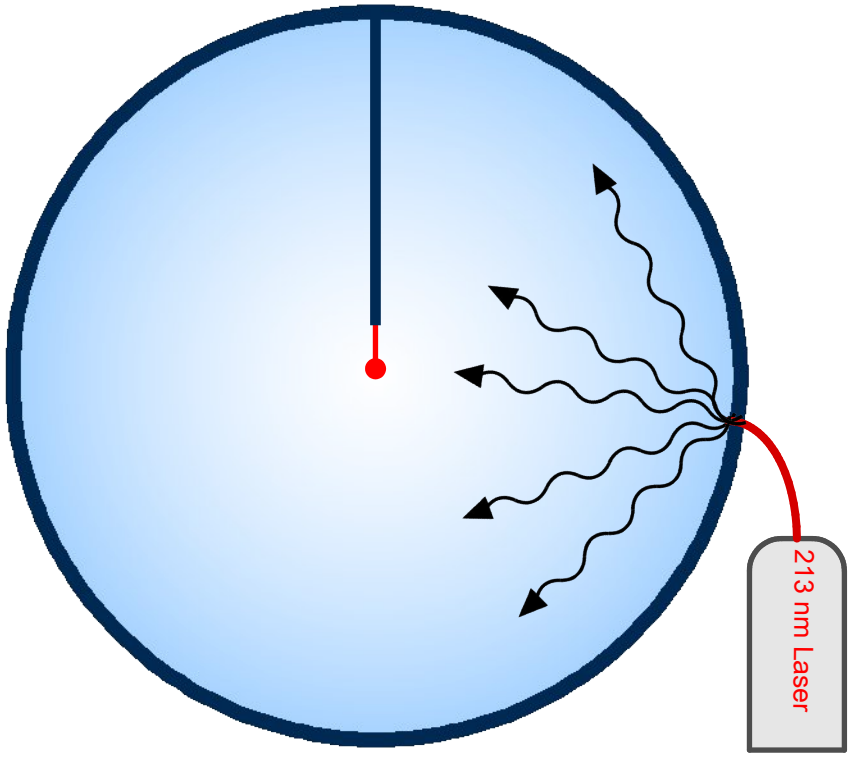

# Thank you!

**Queen's University Kingston - G Gerbier**, P di Stefano, R Martin, G Giroux, S Crawford, M Vidal, G Savvidis, A Brossard, F Vazquez de Sola, Q Arnaud, K Dering, J McDonald, M Chapellier, A Ronceray, P Gros, A Rolland, C Neyron, JF Caron
- Copper vessel and gas set-up specifications, calibration, project management
- Gas characterization, laser calibration on smaller scale prototypes
- Simulations/Data analysis

**IRFU** (Institut de Recherches sur les Lois fondamentales de l'Univers)/**CEA Saclay** - **I Giomataris**, M Gros, T Papaevangelou, JP Bard, JP Mols
- Sensor/rod (low activity, optimization with 2 electrodes)
- Electronics (low noise preamps, digitization, stream mode)
- DAQ/soft

**LSM** (Laboratoire Souterrain de Modane), IN2P3, U of Chambéry - M Zampaolo, A DastgheibiFard
- Low activity archaeological lead
- Coordination for lead/PE shielding and copper sphere

**Aristotle University of Thessaloníki** - I Savvidis, A Leisos, S Tzamarias
- Simulations, neutron calibration
- Studies on sensor

**LPSC** (Laboratoire de Physique Subatomique et Cosmologie) **Grenoble** - D Santos, JF Muraz, O Guillaudin
- Quenching factor measurements at low energy with ion beams

**Pacific Northwest National Laboratory** - E Hoppe, R Bunker
- Low activity measurements, copper electro-forming

**RMCC** (Royal Military College of Canada) **Kingston** - D Kelly, E Corcoran
- $^{37}$Ar source production, sample analysis

**SNOLAB Sudbury** - P Gore, S Langrock
- Calibration system/slow control

**University of Birmingham** - K Nikolopoulos, P Knights, I Katsioulas, R Ward
- Simulations, analysis, R&D

**University of Alberta** - MC Piro, D Durnford
- Gas purification, data analysis

**Associated labs: TRIUMF** - F Retiere

## The NEWS-G Collaboration
(November 2018)

# Extra Slides

# New frontier in WIMP parameter space

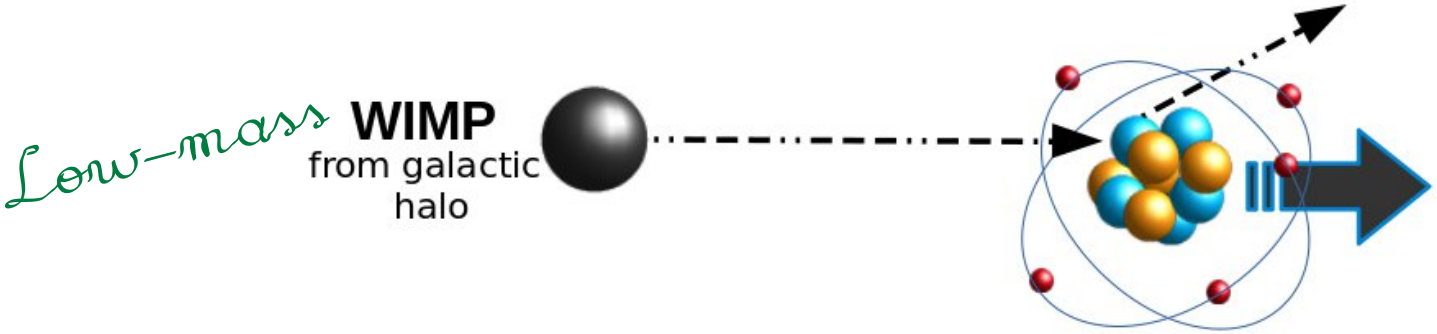


Minuscule energies:
Recoils of $E_R$ ~ 1 keV

→ Low energy threshold

→ Low-A target atom

Neon target, different WIMP masses

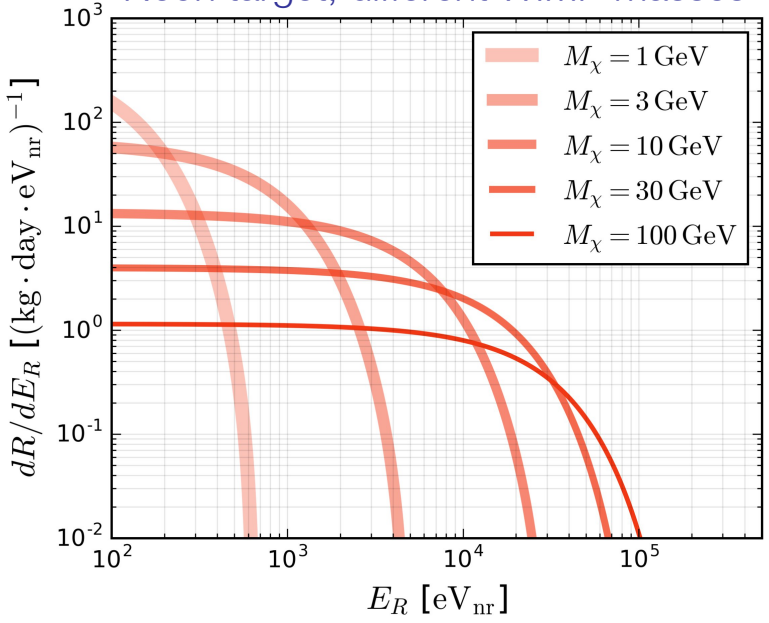


1 GeV WIMP, different targets

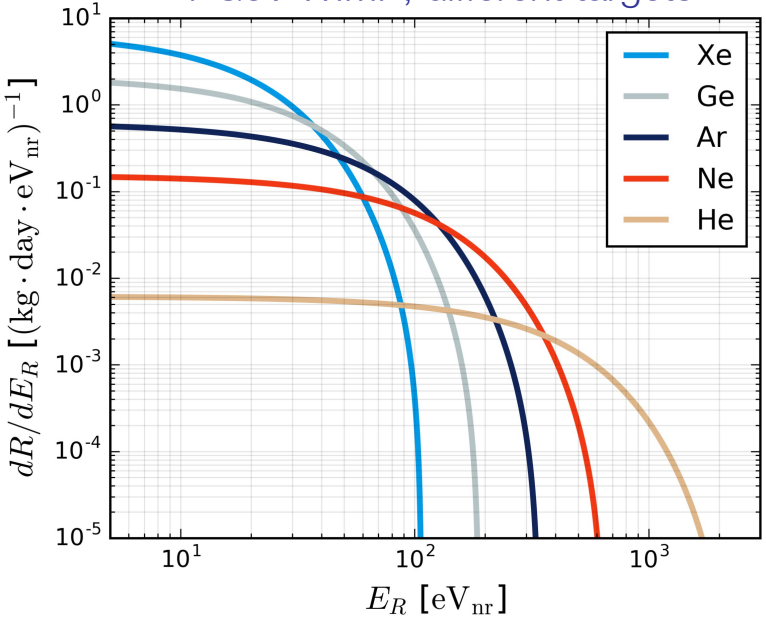

# Principle of operation

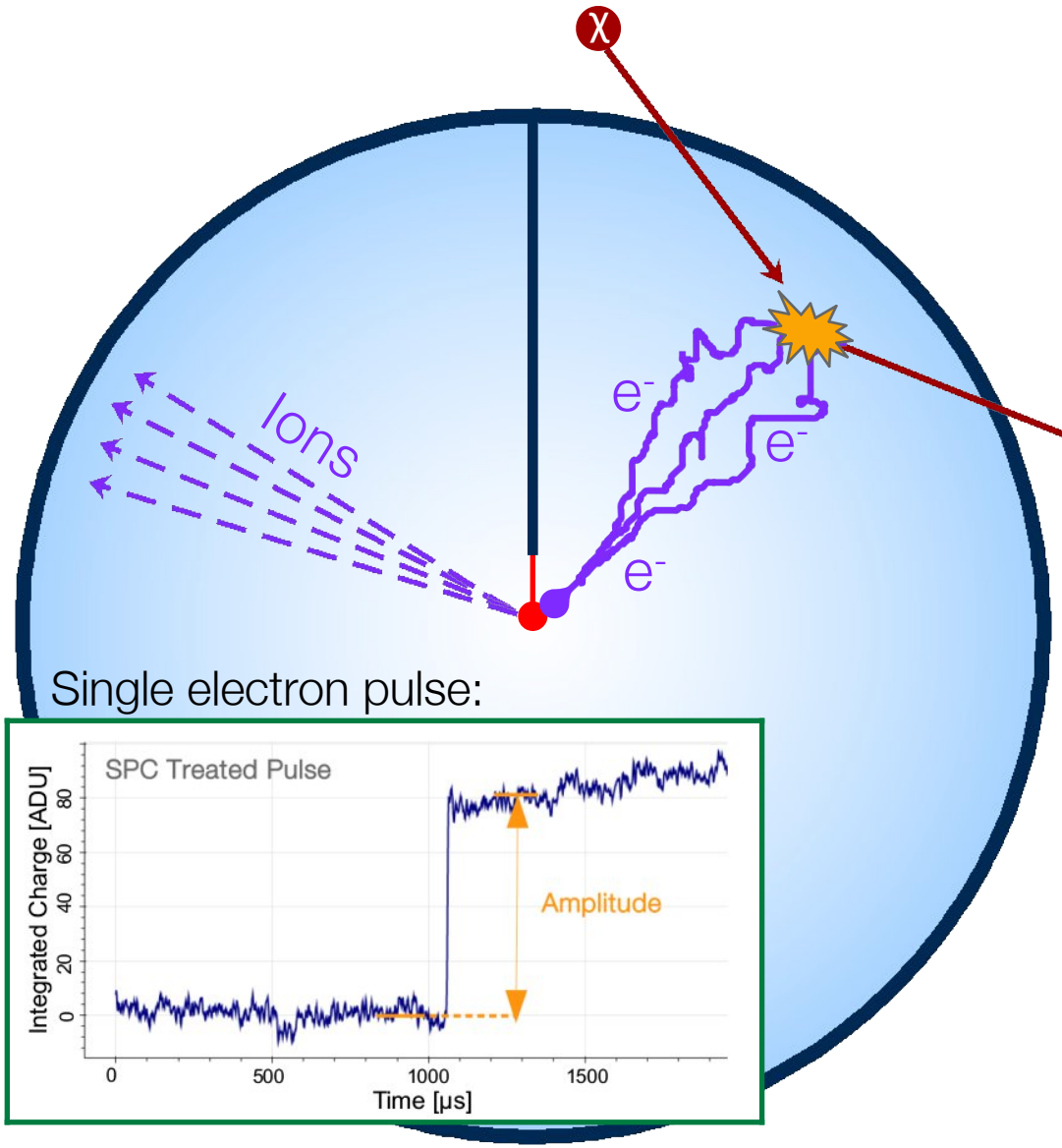


Single electron pulse:




(1) Primary Ionization

$$\langle \#PE \rangle = \frac{E}{W(E)}$$

$$W_{\mathrm{nr}} = W_{\gamma}/Q(E)$$

Neon: $W_\gamma$ ~ 36 eV/pair
Q ~ 0.2

(2) Drift of charges

Typical drift time surface -> sensor :
~ 100 μs

(3) Avalanche of secondary e-/ion pairs

Amplification of signal through
Townsend avalanche (tunable with V)

(4) Signal formation

Current induced by the secondary ions
drifting away from anode

(5) Signal readout

Induced current integrated by a charge
sensitive pre-amplifier and digitized

# Rise time

Gaussian dispersion in arrival time due to diffusion of charges:

$$\sigma(r) = \left(\frac{r}{r_{sphere}}\right)^3 \times 20\mu s$$

Rise time used for surface event discrimination

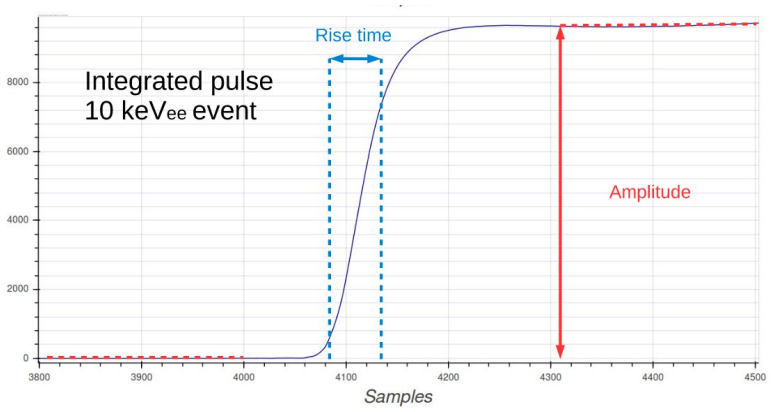


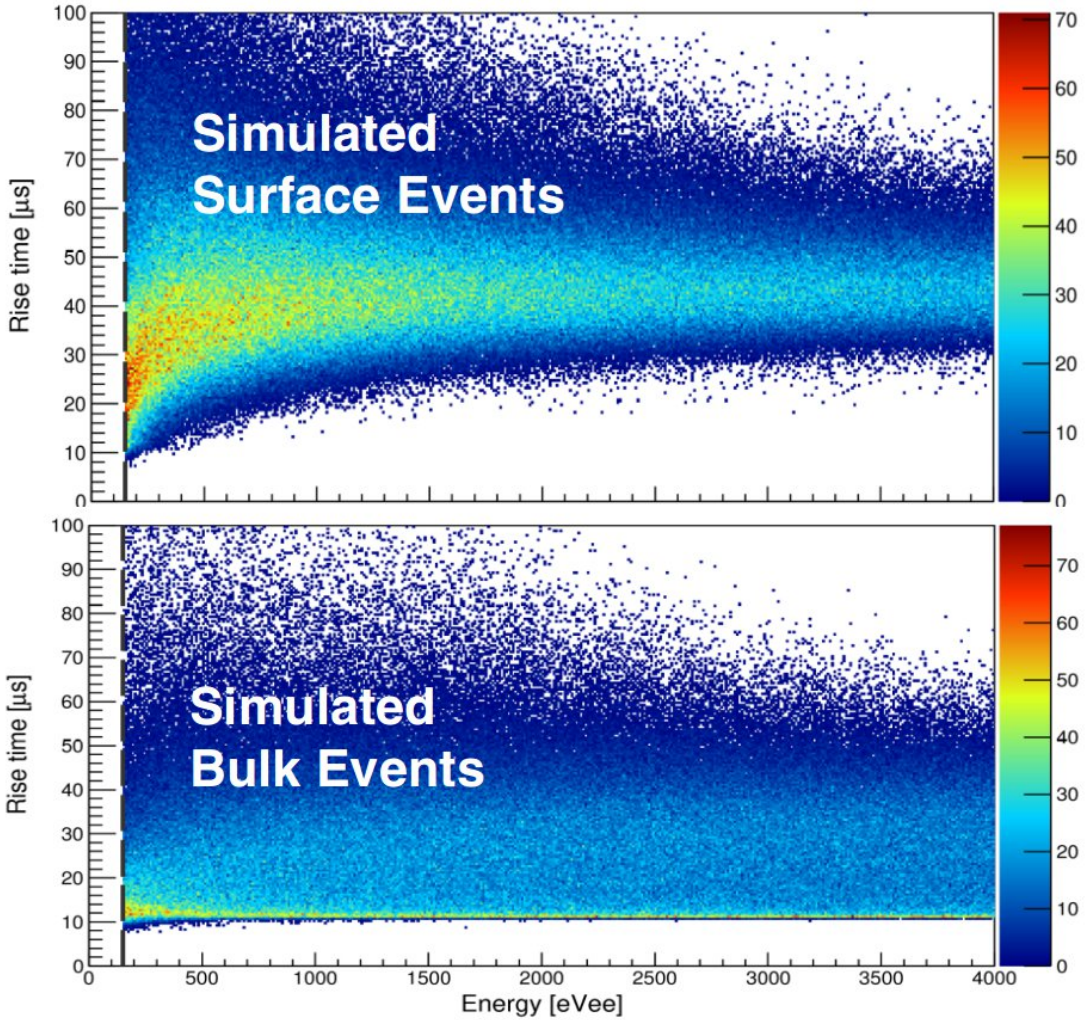


Q. Arnaud et al. (NEWS-G), Astropart. Phys. 97, 54 (2018).

# Event simulation

1) Electric field model from finite element software (COMSOL)

2) Drift of charges simulated with inputs from Magboltz

3) Energy response simulated (see slide 17)

4) Pulses simulated: pre-amp response, ion current, noise

5) Same treatment as real data

Simulated 150 $eV_{ee}$ Event

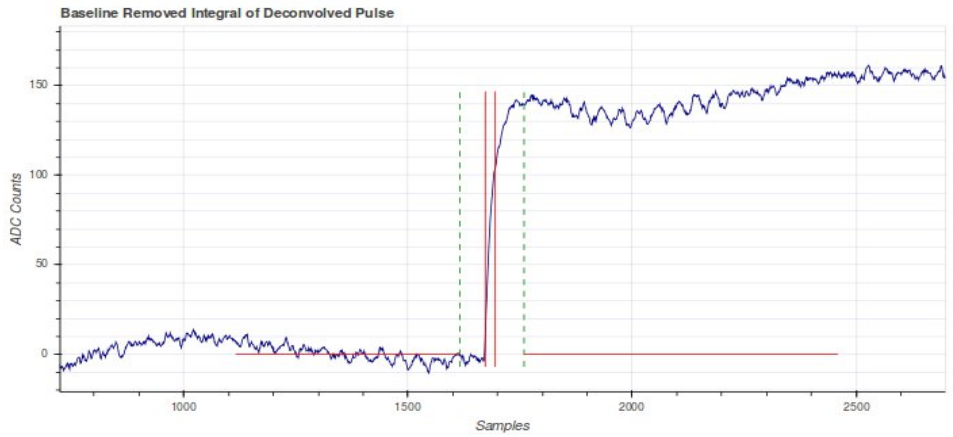


Real 150 $eV_{ee}$ Event

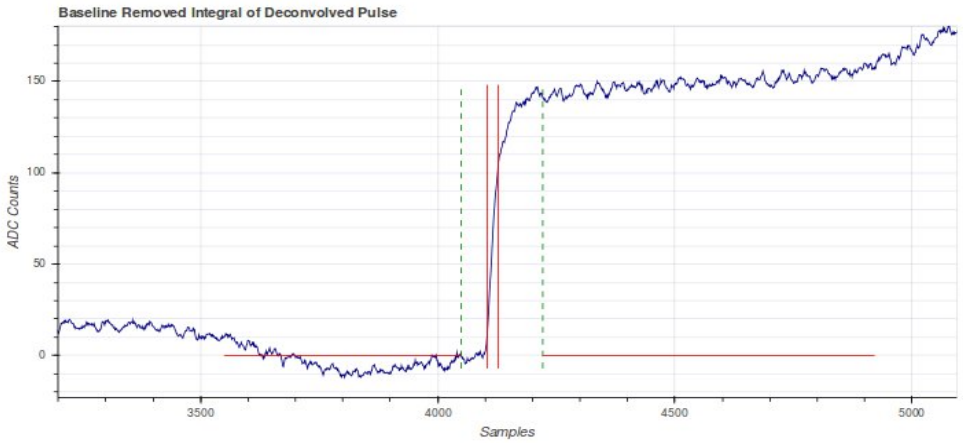

# Event simulation

1) Electric field model from finite element software (COMSOL)

2) Drift of charges simulated with inputs from Magboltz

3) Energy response simulated (see slide 17)

4) Pulses simulated: pre-amp response, ion current, noise

5) Same treatment as real data

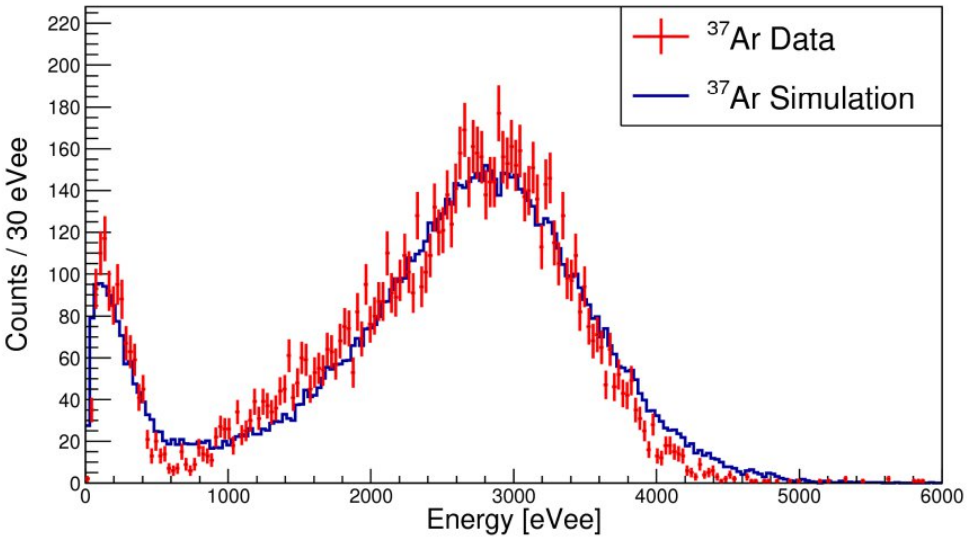


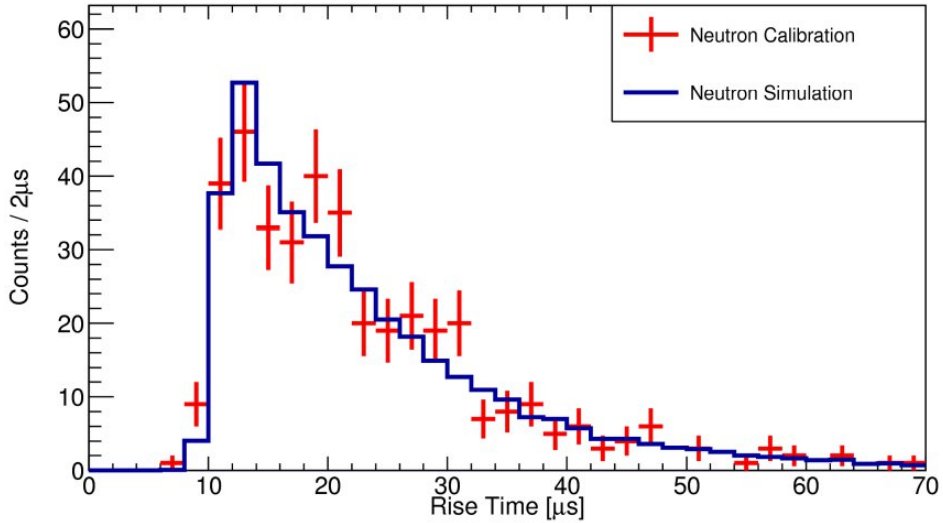

# Pulse treatment

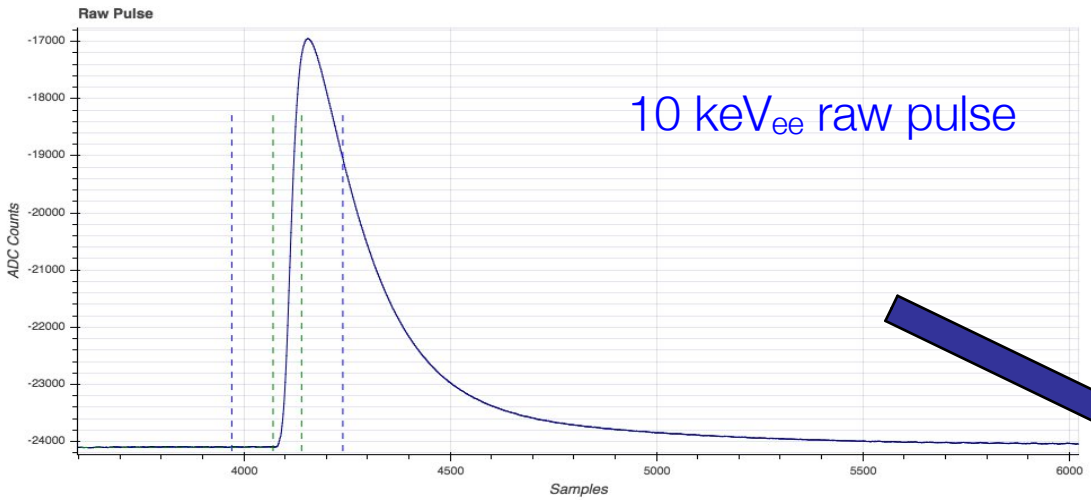


Deconvolve for amplifier response and ion-induced current

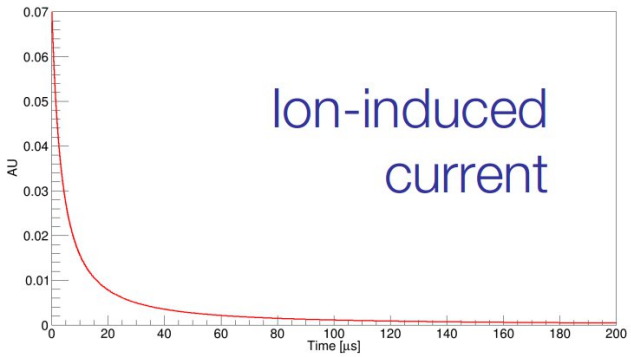


X

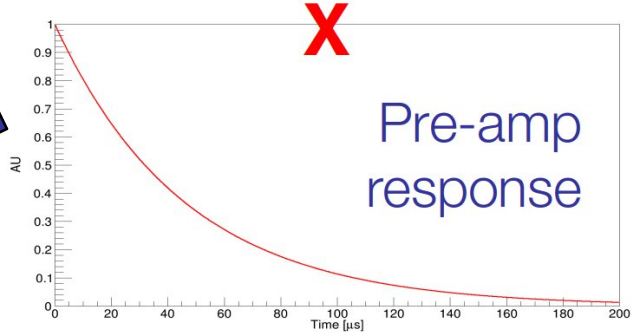


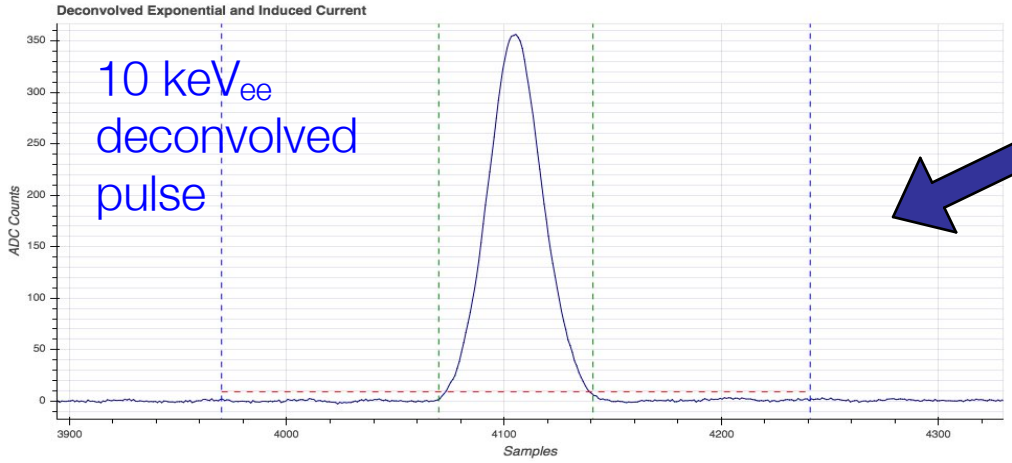

# Detector response model

Analytical model of detector energy response:

$$\frac{dR}{dE}(E_{ee}) = \int_0^{E_{\max}} \frac{dR}{dE}(E_{nr}) \times \sum_{N=0}^{N_{\max}} \left[ P_{\mathrm{COM}}\left(N|\mu, F\right) \times P^{(N)}_{\mathrm{Polya}}\left(E_{ee}|\theta, \langle G \rangle\right) \right] dE_{nr}$$

$$N_{\max} = \left\lfloor \frac{E_{nr}}{I} \right\rfloor \qquad \mu = E_{nr} \times \left( \frac{Q(E_{nr})}{W(E_{nr})} \right)$$

Using the COM-Poisson distribution for primary and Polya for secondary ionization:

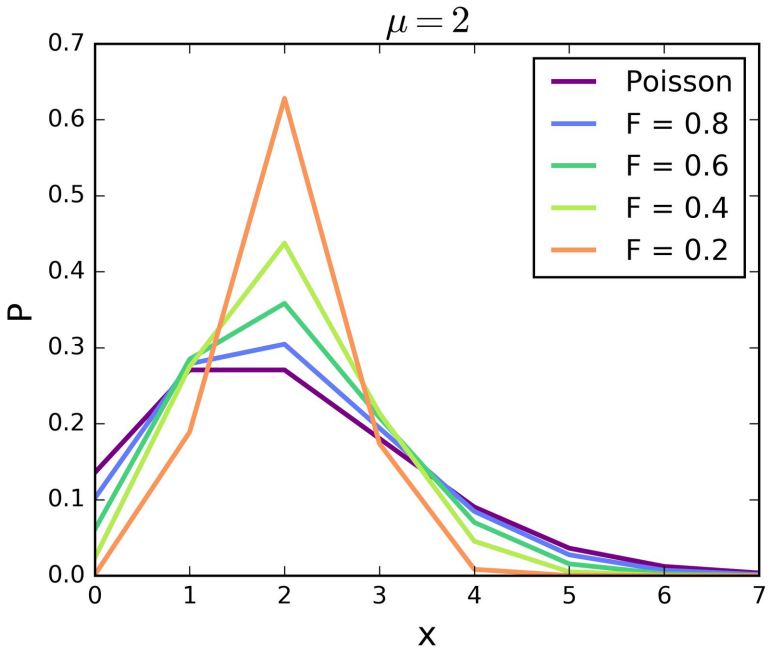


D. Durnford et al. Phys. Rev. D98, 103013 (2018)

$$P(x|\lambda,\nu) = \frac{\lambda^x}{(x!)^\nu \, Z\left(\lambda,\nu\right)}$$

$$Z\left(\lambda,\nu\right) = \sum_{j=0}^{\infty} \frac{\lambda^j}{(j!)^\nu} \qquad \lambda \in \{\mathbb{R} > 0\}, \quad \nu \in \{\mathbb{R} \geq 0\}$$

# Accounting for the Fano factor

We can use this tool to assess the impact on low-mass DM experiments

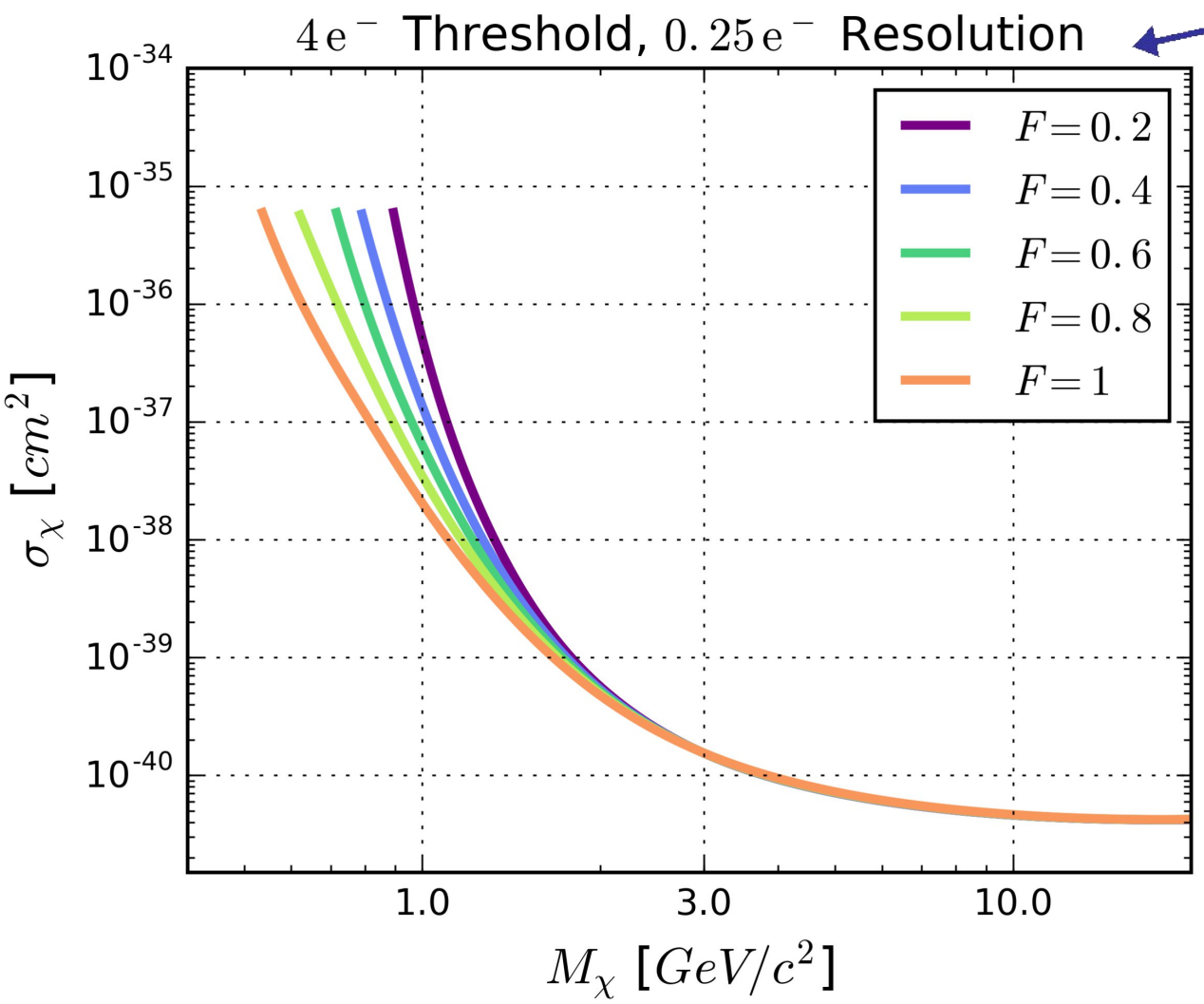


(i.e. CCD detectors like DAMIC)

F can have a big impact!

Neon experiment modelled with COM-Poisson + Gaussian resolution

# Accounting for the Fano factor

We can use this tool to assess the impact on low-mass DM experiments

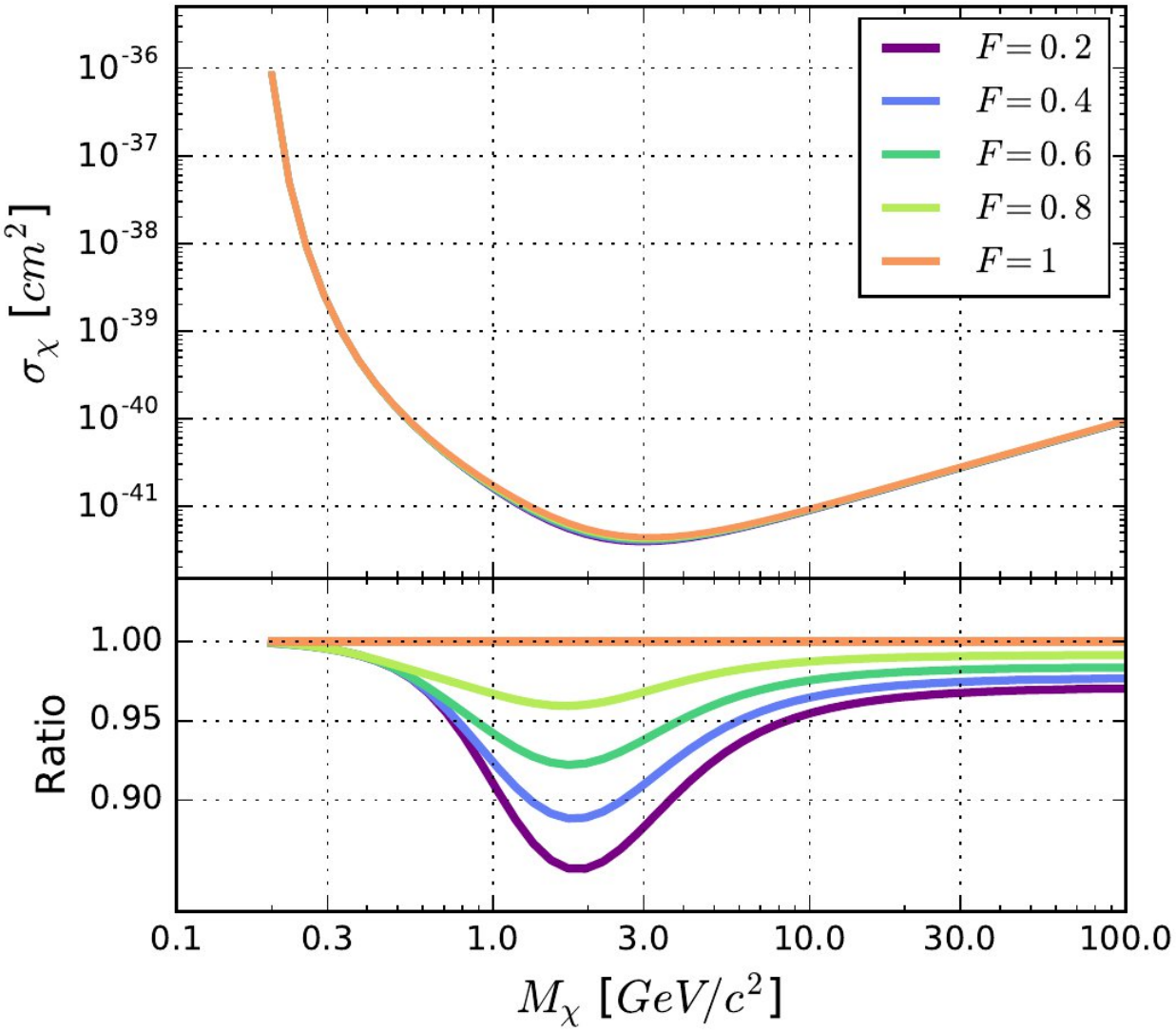


...but probably won't for NEWS-G

Neon experiment modelled with COM-Poisson + Polya, $1e^-$ to 1 $keV_{nr}$ energy window

# The Polya distribution

Modeling of the detector response to single electrons

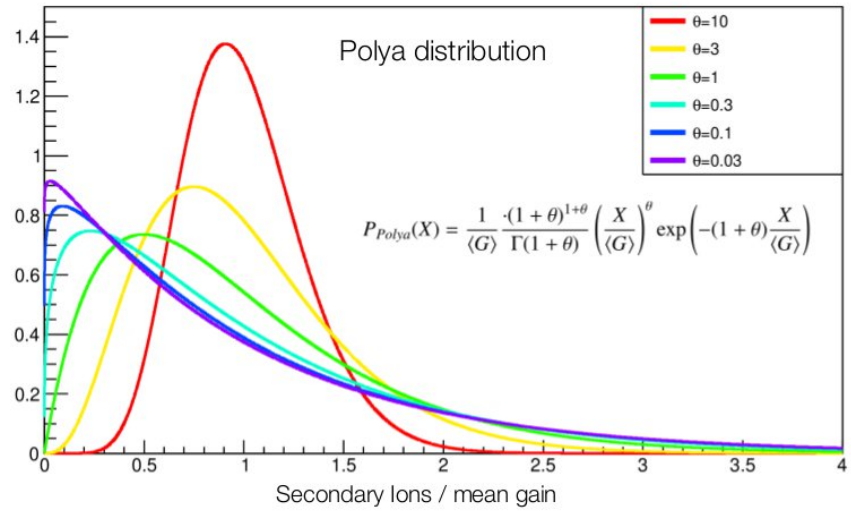


Modeling of the detector response to **N** electrons

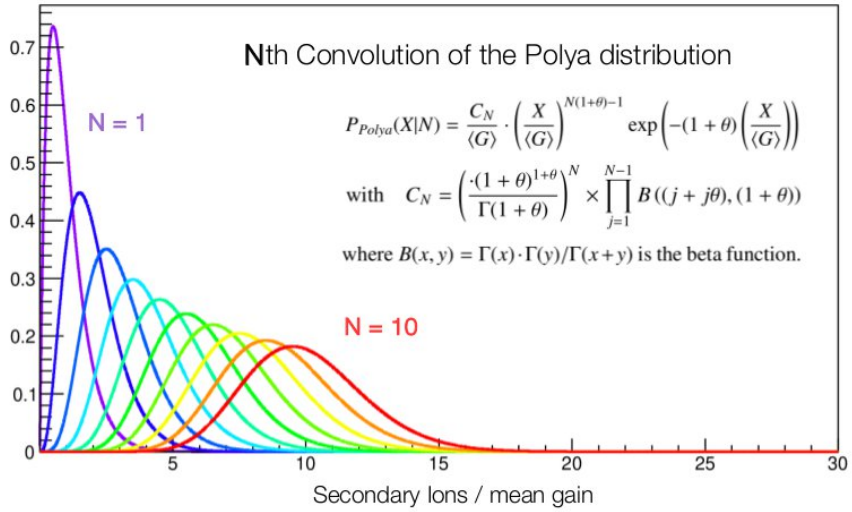


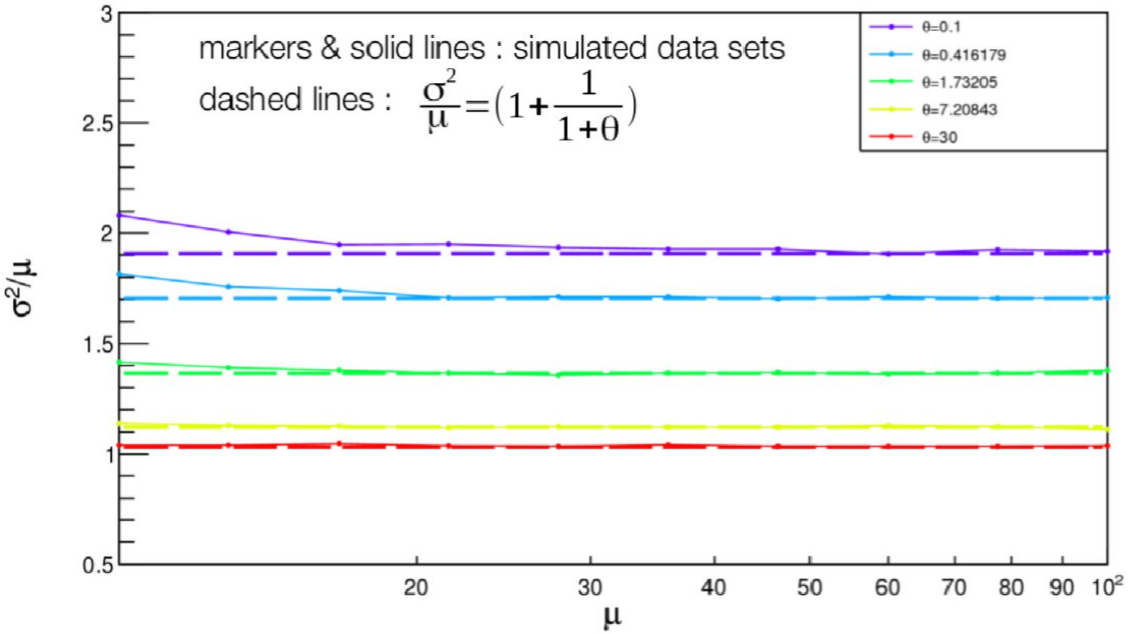


$$\sigma^2 = \sigma^2_{Ionization} + \sigma^2_{Polya}$$

$$\sigma^2 = F\mu + \frac{\mu}{1+\theta} = \mu\left(F + \frac{1}{1+\theta}\right)$$

# Laser power fluctuations

The laser power varies *O*(10%) from pulse to pulse

We deal with this problem by dividing data into subsets with fixed photo-detector amplitude ±5%

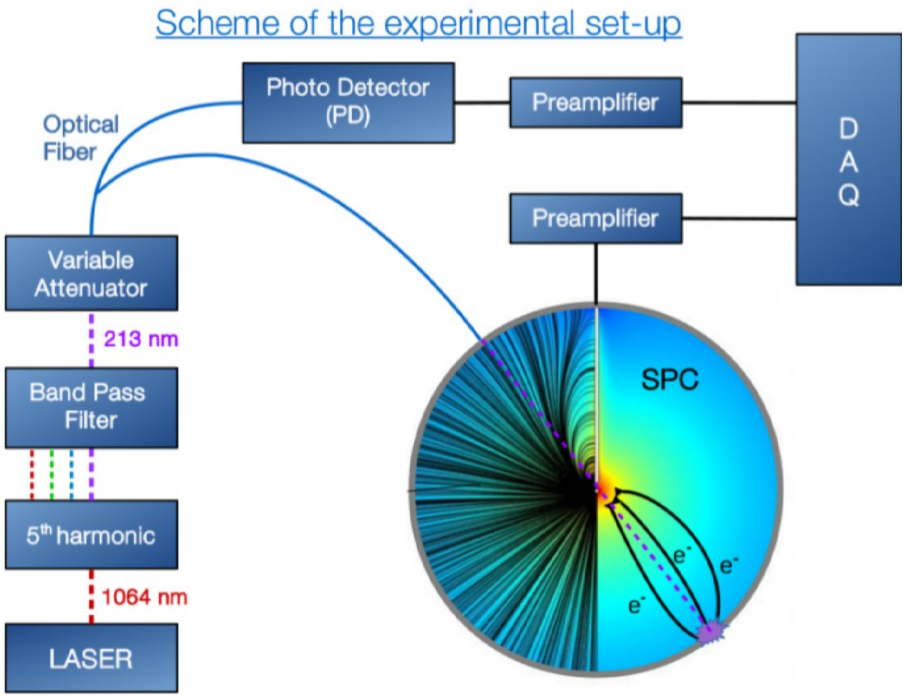


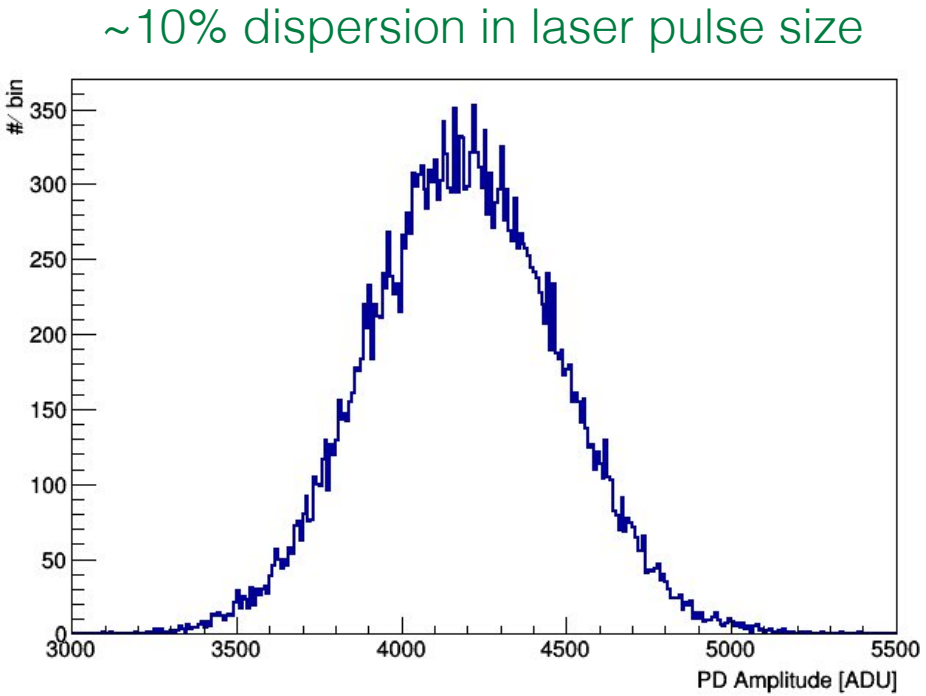

# Laser power fluctuations

The laser power varies *O*(10%) from pulse to pulse

We deal with this problem by dividing data into subsets with fixed photo-detector amplitude ±5%

We disentangle the photo-detector resolution from laser power fluctuations by testing against a second photo-detector

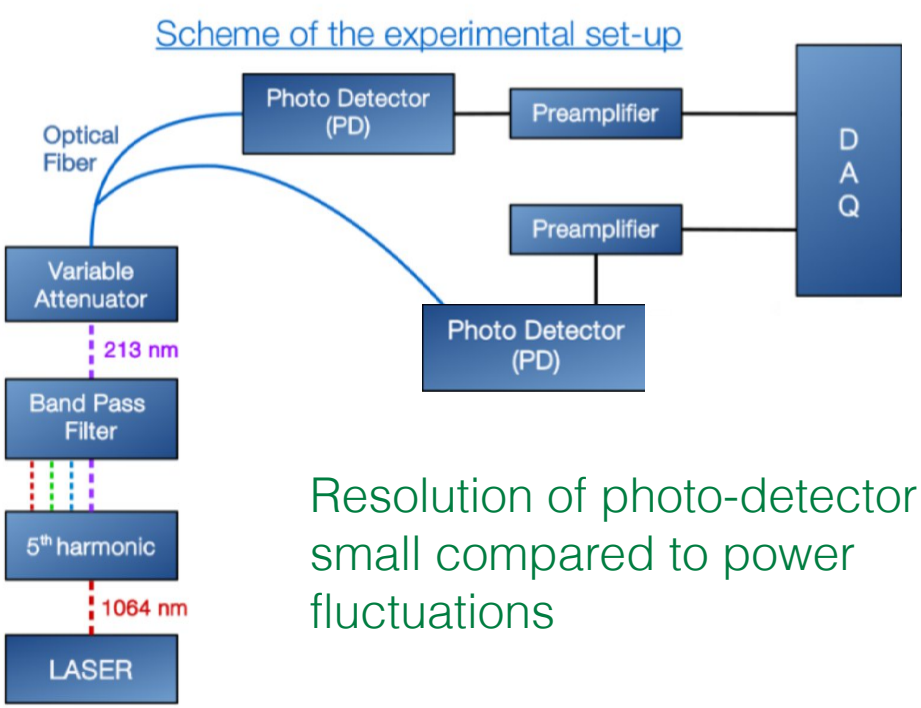


Resolution of photo-detector is small compared to power fluctuations

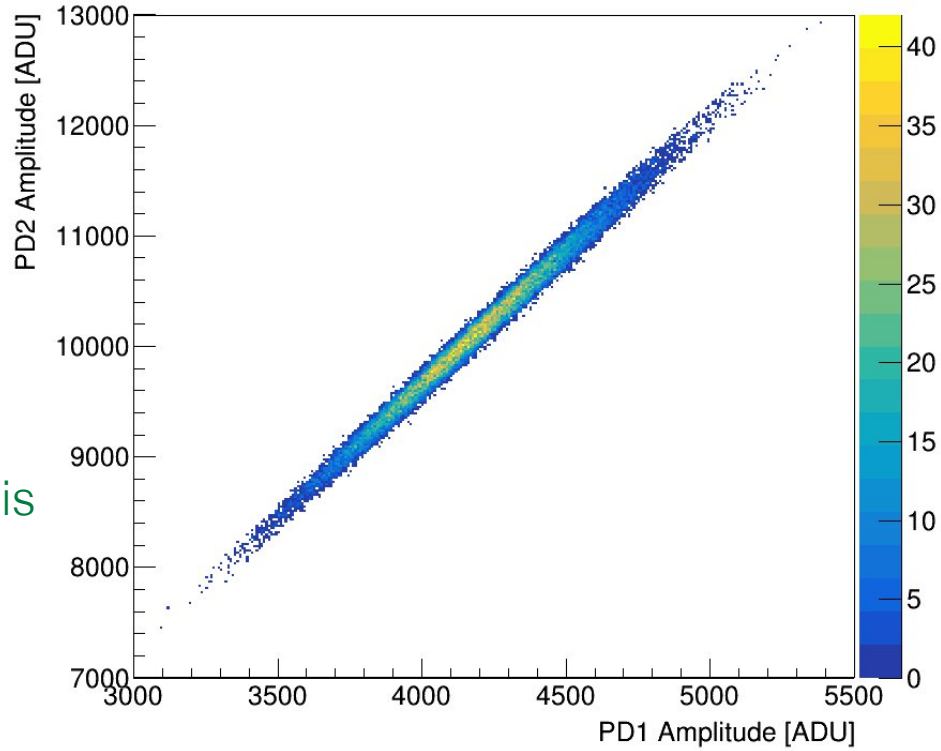

# Data with varying laser intensity

This allows for combined fitting of data subsets, as well as data with different laser intensities:

## Individual Fits

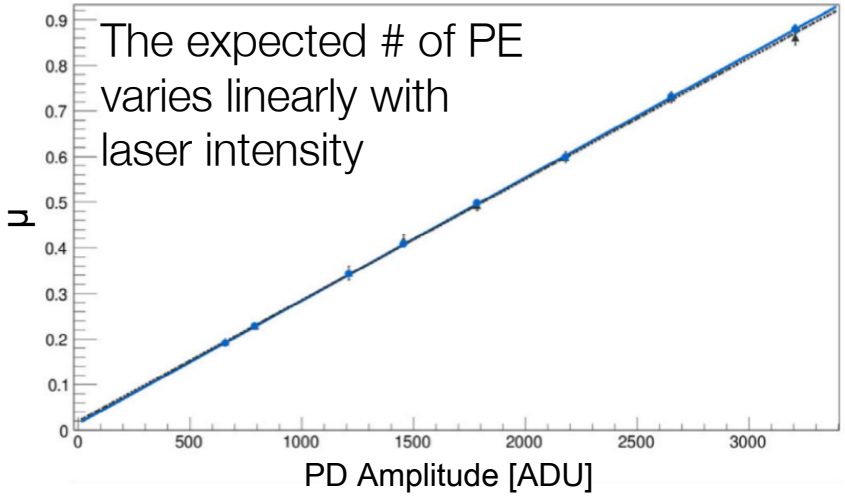


## Joint Fits

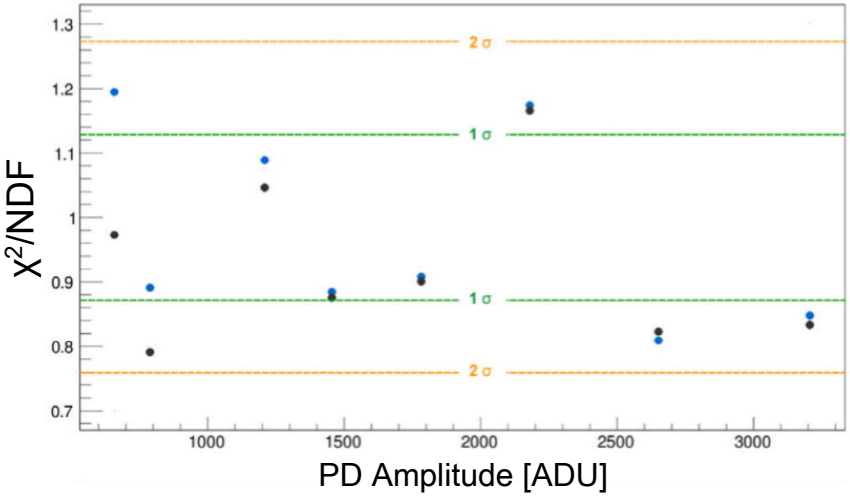


Single and joint fits are in agreement

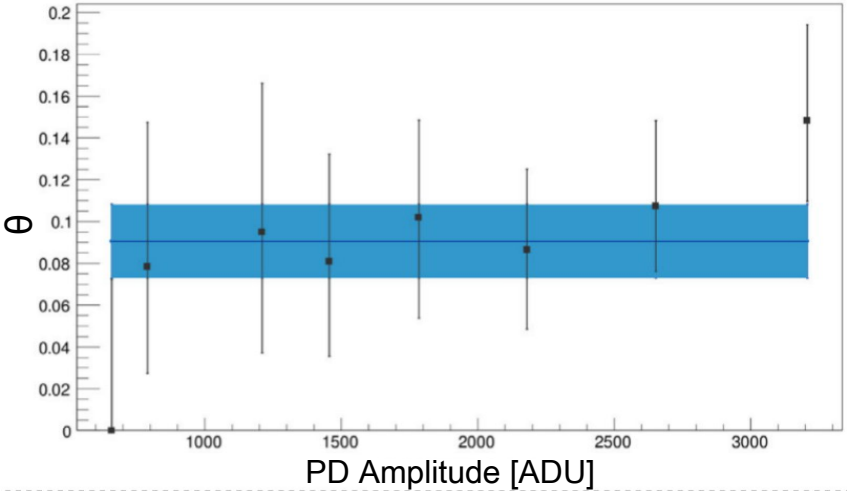


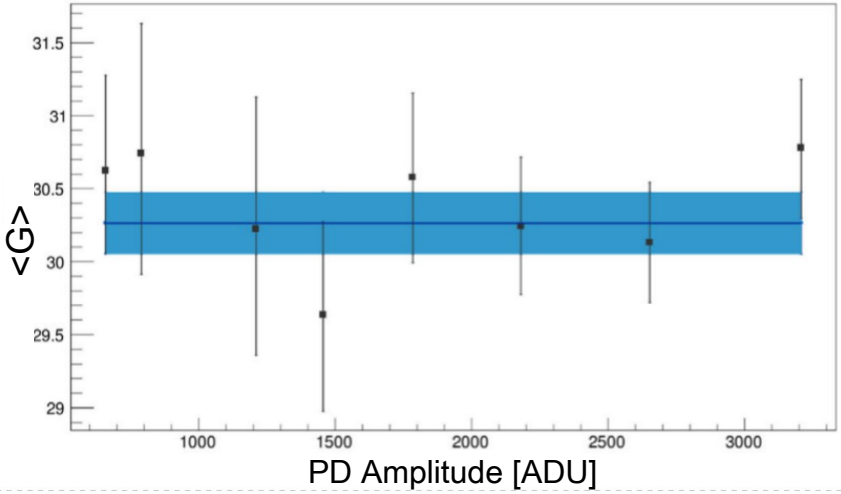


Q. Arnaud et al. (NEWS-G), Phys. Rev. D 99, 102003 (2019)

# Subdividing data sets

To assess the systematic uncertainty associated with the non-fixed value of mu

```
Simulate 1000 MC (toy data sets) {
        For each MC, Simuate 1e6 events{
                For each event{
                    Amplitude simulated with fixed Gain, theta and sigma
                    but with mu drawn randomly between 95% and 105% of mu
                }
        }
        Fit the data and save best fit values
}
```

Distribution of best fit values

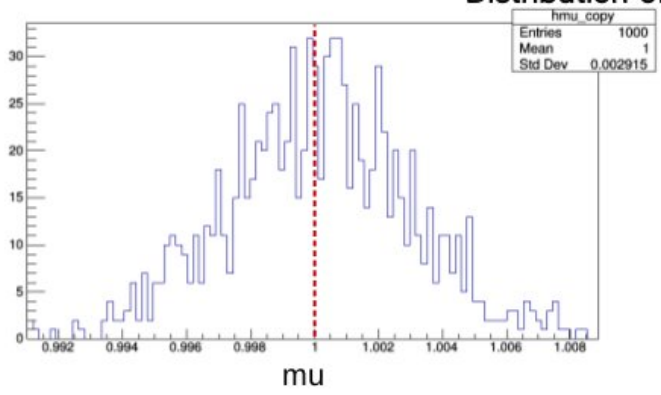


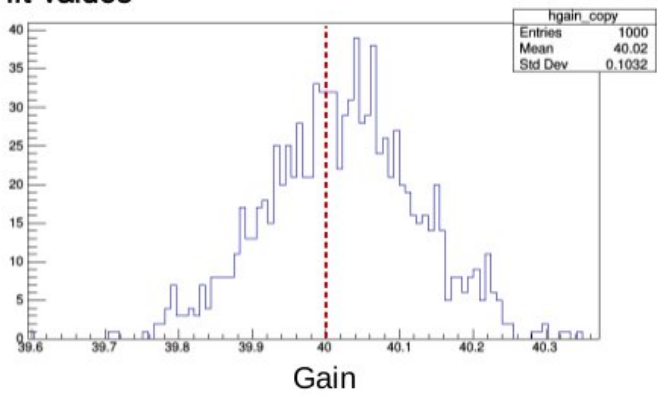


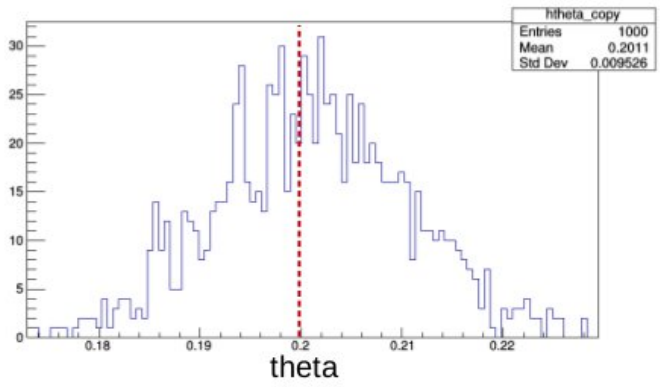


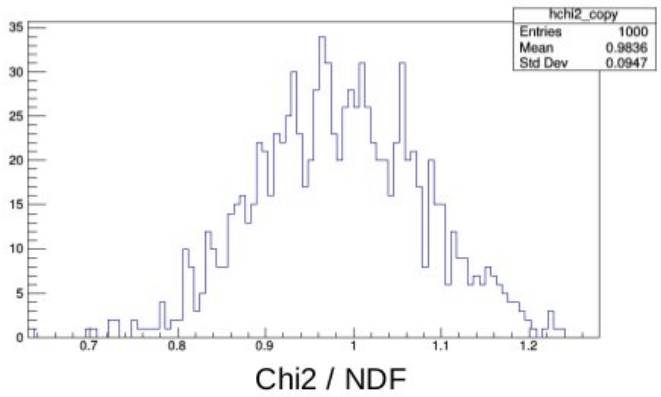

# Subdividing data sets

**Assess the systematic uncertainty associated with non-fixed mu**

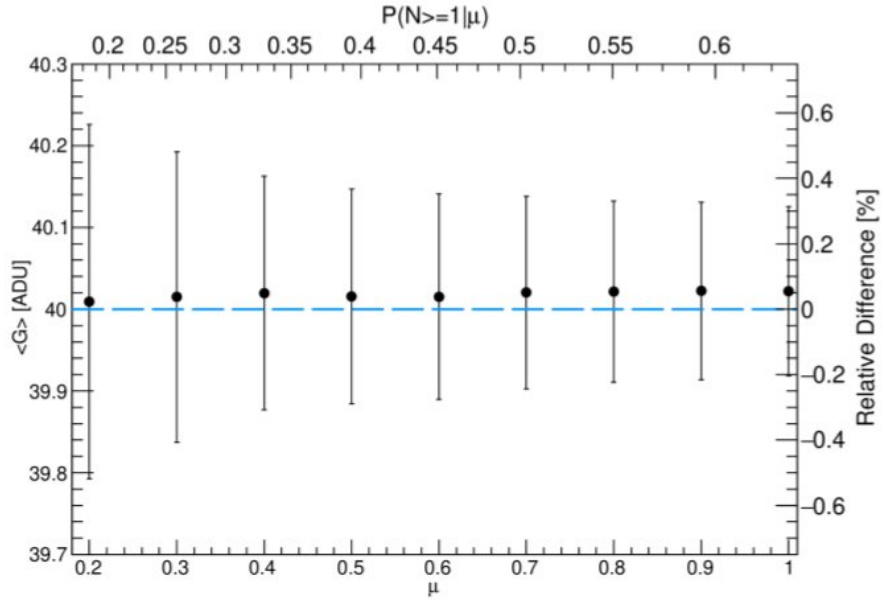


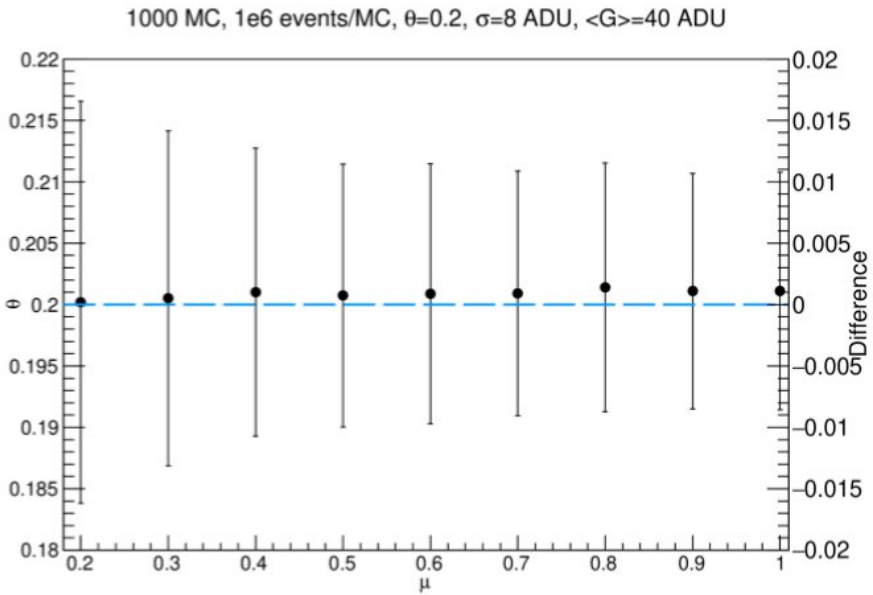


The bias induced by +-5 % fluctuations of mu on the reconstruction of the mean gain is extremely small

$$\frac{P(N|\mu(1+\epsilon))+P(N|\mu(1-\epsilon))}{2} \sim P(N|\mu)\times\left(1+\frac{\epsilon^2}{2}(N^2-3N+1)\right)$$

For +- 5 % fluctuations :

$$\frac{P(N|1.05\mu)+P(N|0.95\mu)}{2} \sim P(N|\mu)\times(1+0.00125\times(N^2-3N+1))$$

# Varying field strength

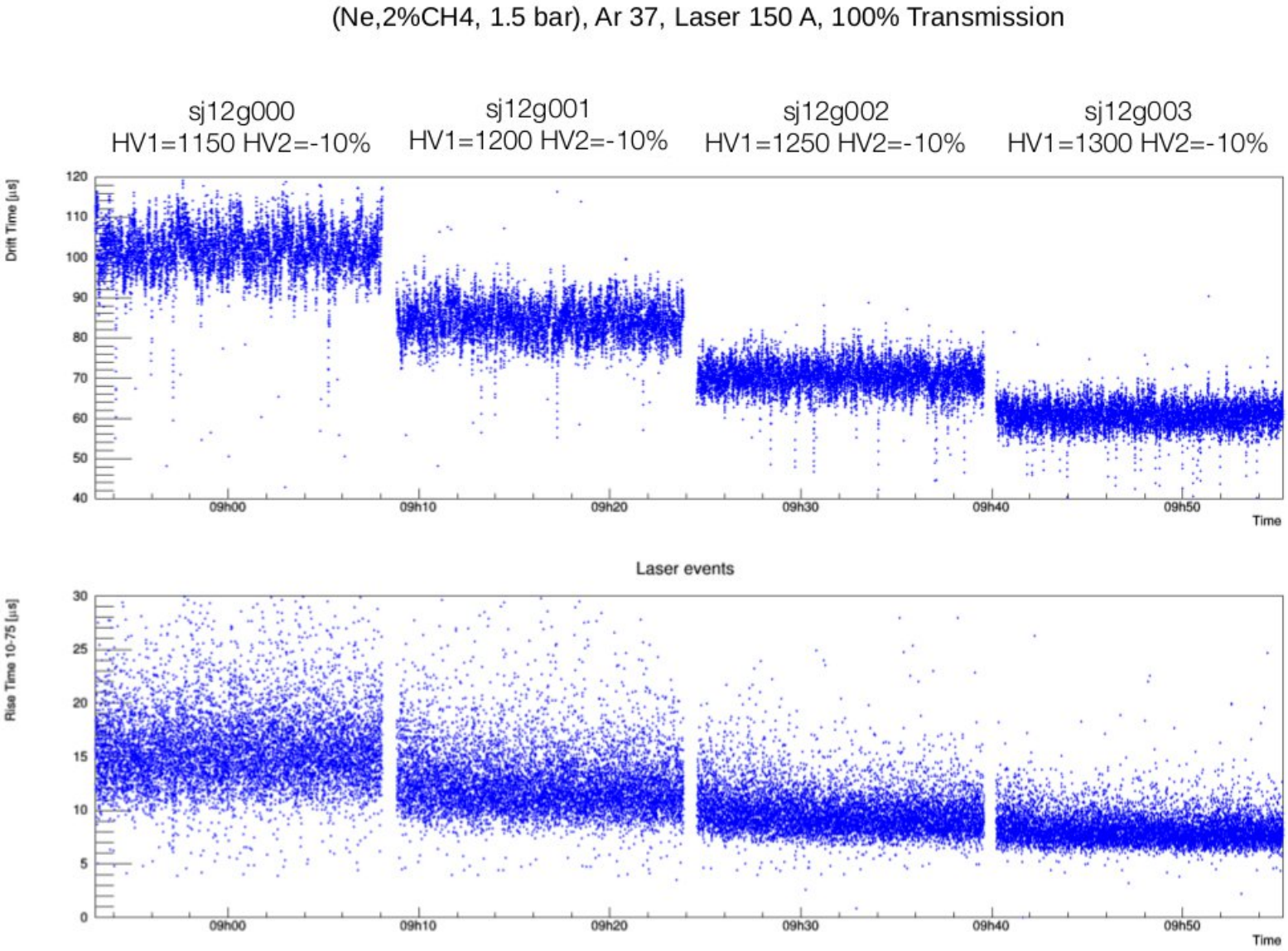


Increase of HV1 -> increase of the field -> Decrease of drift time and diffusion time (as expected)

# Production of $^{37}$Ar

Collaborators at the RMCC produce samples with a fission reactor:

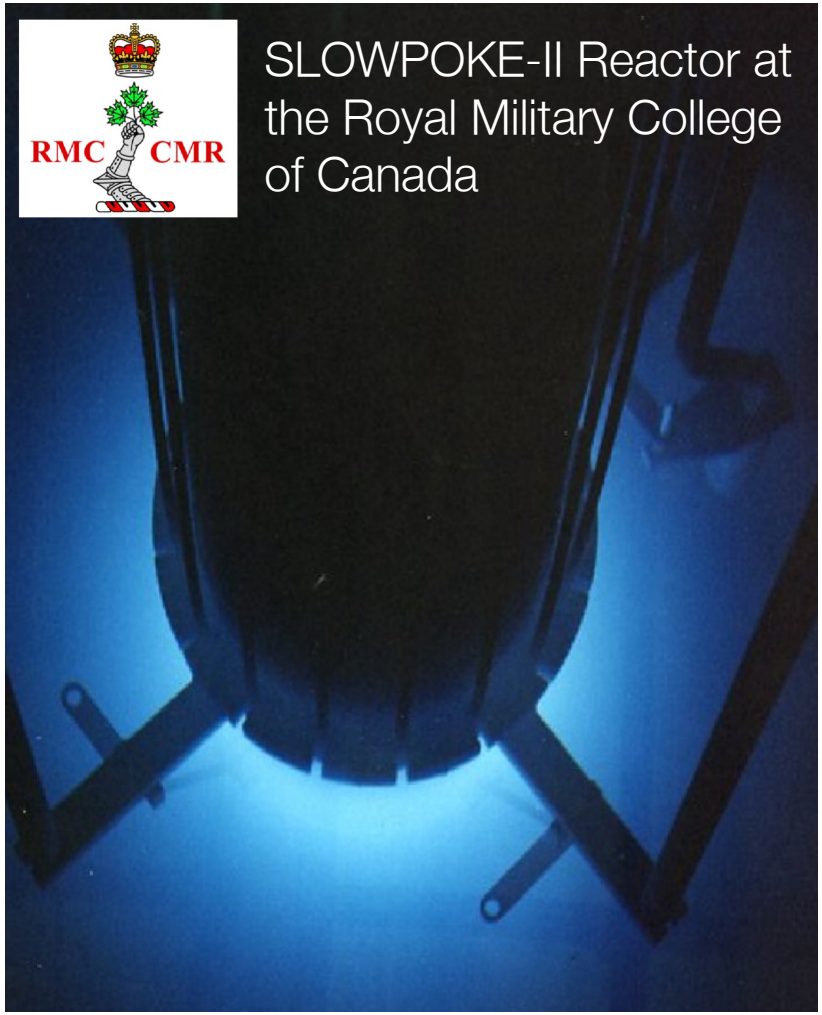


$^{40}Ca(n,\alpha)^{37}Ar$

Source produced in an oxygen-free environment

Counting of gaseous and solid by-products allows for indirect measurement of $^{37}$Ar production

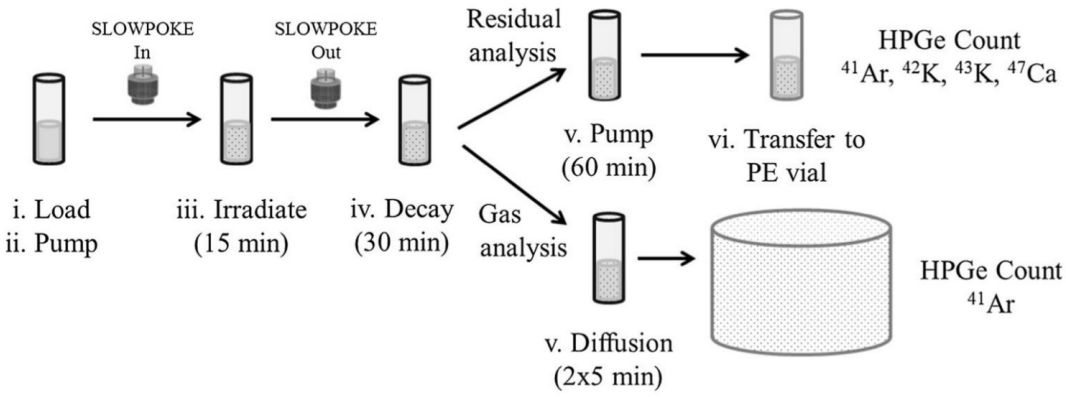


D.G. Kelly et al. Journal of Radioanalytical and Nuclear Chemistry 318(1), 279 (2018).